Bifunctional Charge Transfer Operated Fluorescent Probes with Acceptor and Donor Receptors. 1. Biphenyl-Type Sensor Molecules with Protonation-Induced Anti-Energy Gap Rule Behavior

U. Resch-Genger,*[,†] Y. Q. Li,[†,‡] J. L. Bricks,[§] V. Kharlanov,[||] and W. Rettig*[,||]

Working Group Optical Spectroscopy, Federal Institute for Materials Research and Testing (BAM), Richard-Willstaetter-Strasse 11, D-12489 Berlin, Germany, National Nanotechnology Laboratory, Lecce University, Distretto Tecnologico, Via Arnesano Km 5, 73100 Lecce, Italy, Institute of Organic Chemistry, National Academy of Sciences of the Ukraine, Murmanskaya 5, 235660 Kiev-94, Ukraine, and Institut für Chemie, Humboldt Universität zu Berlin, Brook-Taylor-Strasse 2, D-12489 Berlin, Germany

On the basis of biphenyl (b) type molecules bpb-R substituted with a 2,2′:6′,2″-terpyridine acceptor (bp) and either amino-type donor receptors (R = dimethylamino (DMA), A15C5 = monoaza-15-crown-5) or nonbinding substituents (R = CF$_3$, H, OMe) of various donor strengths, we developed a family of charge transfer (CT) operated monofunctional and bifunctional fluorescent sensors for protons and metal ions. These molecules are designed to communicate the interaction of an analyte with the acceptor and the donor receptor differing in basicity and cation selectivity by clearly distinguishable spectral shifts and intensity modulations in absorption and in emission as well as in fluorescence lifetime. From the dependence of the fluorescence spectra, fluorescence quantum yields, and fluorescence lifetimes of bpb-R on solvent polarity and proton concentration, the photophysics of bpb-R and their protonated analogues can be shown to be governed by the relaxation to a CT state of forbidden nature and by the switching between anti-energy and energy gap law type behaviors. This provides the basis for analytically favorable red shifted emission spectra in combination with comparatively high fluorescence quantum yields. Accordingly, bpb-H and bpb-OMe are capable of ratiometric emission signaling of protons. bpb-DMA reveals a protonation-induced ON–OFF–ON switching of its emission.

1. Introduction

The miniaturized dimensions and high degree of control of molecular design offered by chemical synthesis render organic molecules attractive candidates for molecular electronics and photonics, especially for digital processing and communication.[1] This includes molecular and supramolecular devices, the optical properties of which can be switched or modulated by external stimuli such as chemical,[2–4] electrochemical,[5] thermal,[6] or optical[7] inputs thereby producing a detectable signal, in some cases even on a single molecule level.[8] Such systems can be obtained by combining specific components suitably arranged and connected via either covalent bonds or intermolecular interactions with the interplay of the elementary acts performed by the respective modules determining the device's function. For fluorescence-based analyte recognition of, e.g., either beneficial or harmful metal ions[2,9]—as well as for molecular-scale information processing—molecular systems are desired that combine the ability to recognize and respond to an external input with mediation of a photoinduced electron transfer (ET), charge transfer (CT), or energy transfer process as a mode of signal transduction.[10] Efficient fluorescent probes that are of composite design can be realized by combination of an auxochrome generating the fluorescence signal with an analyte-responsive receptor via either a saturated or an unsaturated spacer.[11] For these molecules, the photophysical process(es) engaged in fluorophore relaxation and the nature of the receptor–fluorophore interactions determine whether the fluorescence signal is modified in intensity and lifetime and/or in energy as response to an external trigger.[12] The latter is the prerequisite for the analytically favorable measurement of the analyte concentration from the ratio of the fluorescence intensities at two different wavelengths that provides an increase in dynamic range and a built-in correction for environmental effects via signal ratioing. However, despite its obvious advantages, ratiometric emission sensing has been scarcely realized for metal ions.[13] Prerequisites here are typically fluoroionophores with two emitting states, the population of which is analyte-controlled. This is found, e.g., in molecules with monomer and excimer (or exciplex) fluorescence[14,15] or in accordingly designed CT-operated probes[16] as well as in certain tautomeric systems[17] or chemodosimeters[18] that are, however, beyond the scope of this article.[19] For CT-operated sensor molecules, cation-triggered spectral shifts in emission—and thus prevention of cation photorelease or deco-ordination in the excited state[20]—can be realized with a variety of design concepts. Comparatively rare examples of such ratiometric systems include donor (D)–acceptor (A) substituted molecules with acceptor-type binding sites[21–23] or participation of the electron-accepting chromophore in analyte coordination,[24] analyte-mediated transformation of a donor receptor into an acceptor in D–D substituted sensor molecules,[25,26] or combination of two CT processes in a more complex D¹–A–D² type design.[27,28] Acceptor coordination that is the most straightforward strategy toward analyte-triggered red shifts in emission and ratiometric signaling, however, relies on suitable electron-

---
† BAM.
‡ Lecce University.
§ National Academy of Sciences of the Ukraine.
|| Humboldt Universität zu Berlin.

accepting receptors that can be integrated into fluorophore π-systems and on the formation of at least moderately fluorescent acceptor chelates in polar solvents. The realization of the latter requires insight into the photophysical mechanisms involved in fluorophore relaxation in the probe's neutral, i.e., uncomplexed, and ionic or charged, i.e., complexed, state and eventually tuning of the fluorescence properties of acceptor-coordinated systems by proper choice of the strength of donor and acceptor substituents. Accordingly, the knowledge of the structure−property relationship of the respective dye class and its ionic counterparts plays an important part in the rational design of fit-for-purpose sensor molecules.

Aside from consideration of the prerequisites for input-triggered intensity and energy modulations in absorption and emission, the ever-increasing interest in the application of fluorescent probes and switches as advanced sensory and molecular-scale information processing devices favors multi-functional systems that contain more than one receptor and/or reporter unit and undergo clearly distinguishable changes of different measurable fluorescence parameters specific for certain chemical inputs.[29,30] This permits, for instance, simultaneous and/or cooperative sensing of different species or consecutive signaling of a single analyte at different concentration regimes at the same location.[28,31,32] Also advantageous here is a composite constitution that allows tuning of the device's sensitivity and selectivity by proper choice of functional components. However, rationalization of bi- and multifunctional systems imposes strict requirements on suitable design concepts including receptor modules. At present, the majority of bifunctional molecules or devices with logic action respond to combinations of protons and alkali or alkaline earth metal ions and are ET-operated, i.e., limited to intensity alterations.[33] There are only a few examples known for CT-operated molecules as well as for systems signaling transition metal ions.[28,34,35]

As an extension of our work on ET- and CT-operated fluorescent probes and neutral and ionic donor (D)−acceptor (A) biphenyls, we designed a family of proton responsive and metal ion responsive biphenyl-type molecules. These mono- and bifunctional sensor molecules are substituted with different acceptor-type receptors and coordinating or noncoordinating donor substituents as a prerequisite for tuning of their D−A strength, functionality, and analyte selectivity. The aim was here to conceive structure−property relationships for CT-operated sensor molecules that (i) enable ratiometric emission signaling and (ii) can exist in three or four spectroscopically clearly distinguishable states. Communication of whether *none*, *only one* (equaling little or below a certain concentration threshold), or *both* binding sites (equaling much or above a certain concentration threshold) are bound is the prerequisite for consecutive sensing of a single analyte at different concentration regimes, thus elegantly extending the probe's dynamic range, whereas the simultaneous recognition of two different chemical inputs relies on the indication of whether *none*, *only one*, *the other one*, or *both* binding sites are engaged in analyte coordination. In part 1 of this series, we investigate the ability and structural requirements of the D−A biphenyl-type molecules bpb-R shown in Scheme 1 to serve as proton-sensitive ratiometric fluorescent probes as well as to act as bifunctional fluorescent sensors. bpb-R molecules combine the advantageous properties of D−A substituted biphenyls, i.e., their well-known photophysics,[36−41] D−A strength controlled spectroscopic properties, and their comparatively high fluorescence quantum yield of CT[42] emission[36] with a terpyridine A-type receptor. Terpyridine is chosen here because this common stable tridentate

SCHEME 1: Chemical Structures of bpb-R, Where R = CF₃ (1), H (2), OMe (3), DMA (4), and A15C5 (5)
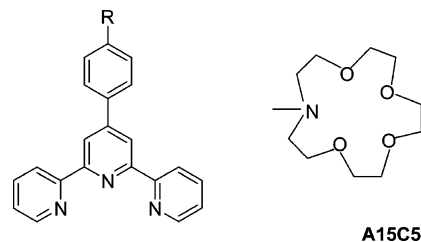
ligand for a broad variety of metal ions[43] and versatile building block for supramolecular assemblies[44] and sensor molecules[45−47] can be readily integrated into D−A biphenyls. Moreover, the basicity or proton affinity of its nitrogen atoms exceeds that of the nitrogen donor substituents in bpb-DMA (DMA = dimethylamino) and bpb-A15C5 (A15C5 = monoaza-15-crown-5), thereby providing the basis for bifunctional proton sensing. Moreover, as detailed in part 2 of this series,[48] the metal ion selectivity and complexation constants of the terpyridine acceptor and the monoaza crown donor receptor are expected to strongly differ. This is the prerequisite for bifunctional cation recognition. The bpb-R series is designed not for real-world analytical applications that commonly require proper functioning in aqueous systems, signaling in the visible/near-infrared spectral region, and selective ligands, but for the systematic study of acceptor vs donor coordination, for the evaluation of design principles for ratiometric emission sensing, and for the realization of bifunctional probes. Accordingly, comparison with other spectroscopically well characterized model systems: see Schemes 2 and 3 for examples, the majority of which have been investigated in acetonitrile. Part 1 of this series focuses on the solvatochromic and photophysical properties of bpb-R and their protonation and alkylation behaviors to derive prerequisites for biphenyl-type molecules that form emissive acceptor chelates and are capable of multimodal analyte signaling. As an extension of the chemosensor studies, additionally the potential of bpb-R as molecular switches and equivalents of logic gates is discussed.

2. Experimental Section

2.1. Materials. All the chemicals used for the synthesis of the probes were purchased from Merck. All the solvents employed were of spectroscopic grade and purchased from Aldrich. Prior to use, all the solvents were checked for fluorescent impurities.

2.2. Apparatus. The chemical structures of the synthesized compounds were confirmed by elemental analysis, ¹H NMR, and ¹³C NMR. Their purity was checked by fluorescence spectroscopy. Melting points (uncorrected) were measured with an IA 9100 digital melting point analyzer (Kleinfeld GmbH), and NMR spectra were obtained with a 500 MHz NMR spectrometer, Varian Unity$_{plus}$ 500. Elemental analyses were performed in duplicate and were carried out at the Institute of Organic Chemistry, National Academy of Sciences of the Ukraine, Kiev, with samples dried prior to analysis for 5−6 h at 80 °C in vacuo following routine procedures.

2.3. Steady-State Absorption and Fluorescence. The UV/vis spectra were recorded on a Carl Zeiss Specord M400/M500 and a Bruins Instruments Omega 10 absorption spectrometer. The fluorescence spectra were measured with a Spectronics Instruments 8100 and a Perkin-Elmer LS 50B spectrofluorometer. Unless otherwise stated, all the fluorescence spectra presented are corrected for the wavelength- and polarization-dependent spectral responsivity of the detection system traceable

10958 *J. Phys. Chem. A, Vol. 110, No. 38, 2006*

Resch-Genger et al.

to the spectral radiance scale. This instrument-specific quantity was determined with a calibrated quartz halogen lamp placed inside an integrating sphere and a white standard, both from Gigahertz-Optik GmbH in the case of the 8100 fluorometer and with spectral fluorescence standards with known corrected emission spectra for the LS50B fluorometer following previously described procedures.[49,50] The emission spectra on a wavenumber scale were obtained by multiplying the measured and corrected emission spectra with λ^2.[51] The absorption and emission maxima given are determined from the respective spectra plotted on an energy scale.

The fluorescence quantum yields (ϕ_f), which were measured with the 8100 fluorometer with Glan Thompson polarizers placed in the excitation channel and emission channel set to 0° and 54.7°, were calculated from integrated, blank, and spectrally corrected emission spectra (wavelength scale; prior to integration multiplication with λ)[50] employing quinine sulfate in 1 N H$_2$SO$_4$ ($\phi_f = 0.55 \pm 0.03$)[52] and coumarin 153 in ethanol ($\phi_f = 0.4$)[53] as fluorescence standards. For each compound–solvent pair, the quantum yield was determined twice. Typical uncertainties of fluorescence quantum yield measurements as derived from previous measurements are ±5% (for $\phi_f > 0.4$), ±10% (for $0.2 > \phi_f > 0.02$), ±20% (for $0.02 > \phi_f > 0.005$), and ±30% (for $0.005 > \phi_f$), respectively.[34]

2.4. Time-Resolved Fluorescence. Fluorescence decay curves were recorded with the time-correlated single-photon-counting technique (TCSPC)[54] using an Ar-pumped Ti:sapphire laser as excitation source and a previously described setup[55] as well as with a similar setup at the Berlin Synchrotron facility BESSY II. The latter employs synchrotron radiation as excitation light source in conjunction with an excitation monochromator (Jobin Yvon, II, 10 UV). BESSY II delivers a 1.25 MHz pulse train with characteristic pulse widths of 30–50 ps. The fluorescence decays were detected with a microchannel plate photomultiplier tube (MCP; Hamamatsu R 1564-U-01) cooled to −30 °C that was coupled to an emission monochromator (Jobin Yvon II, 10 VIR) by means of quartz fiber optics. The signal from a constant fraction discriminator (CFD; Tennelec 454) was used as the start pulse for the time-to-amplitude converter (TAC; Tennelec TC864) operated in the reverse mode. The BESSY II synchronization pulse was applied as the stop pulse. The MCP pulses were amplified by an amplifier (INA 10386) and coupled into the CFD. A multichannel analyzer (Fast Comtec MCDLAP) was employed for data accumulation. The decays were analyzed by the least-squares iterative reconvolution method on the basis of the Marquardt–Levenberg algorithm, which is implemented into the commercial global analysis program.[56] The instrument response function (IRF) that was obtained by the detection of Rayleigh scattered light in a scattering solution had a width of 50–60 ps for the laser setup used and a width of 120 ps in the case of experiments at BESSY II. The quality of the exponential fits was evaluated on the basis of reduced χ^2 values.

2.5. Quantum-Chemical Calculations. Semiempirical ground-state calculations were carried out with the AM1 Hamiltonian[57] within Gaussian 98 and with AMPAC.[58] Full geometry optimization of the ground-state structure of the species under consideration was performed, and minima were checked using the Hessian matrix. For twisted geometries, the corresponding dihedral angle was fixed, and all the remaining variables were fully optimized. The calculations of the transition energies and oscillator strengths were performed with ZINDO/CI in Gaussian 98[59] with configuration interaction of 10 occupied and 10 unoccupied orbitals for the fully optimized AM1 ground-state structures or with AM1/CI (CI = 10).

2.6. Synthesis. The bpb-R series was prepared following literature procedures with the synthesis of bpb-H, bpb-OMe, and bpb-DMA having been previously described.[60−62] The preparation of alkylated bpb-H shown in Scheme 4 has been recently published by some of us.[63]

4′-[4-(Trifluoromethyl)phenyl]-2,2′:6′,2′′-terpyridine (bpb-CF$_3$, 1). In a first step, the starting material for the synthesis of **1**, 1,5-dipyridin-2-yl-3-[4-(trifluoromethyl)phenyl]pentane-1,5-dione (**1a**), was prepared by addition of 0.33 g of an aqueous solution of tetraethylammonium hydroxide (30%) to a solution of 1.6 g (0.013 mol) of 2-acetylpyridine and 1.16 g (0.0065 mol) of *p*-trifluoromethylbenzaldehyde in 5 mL of 2-propanol. This mixture was heated at 60 °C for 1 h and poured into 100 mL of water. The solid was filtered off and recrystallized from 2-propanol and from cyclohexane. Yield: 1.3 g (42.1%). mp 103−105 °C. Elemental analysis, found: C, 66.29; H, 4.17; N, 7.12. Calcd for C$_{22}$H$_{17}$F$_3$N$_2$O$_2$: C, 66.32; H, 4.30; N, 7.03. ^{1}H NMR (CDCl$_3$, 300 MHz) δ (ppm): 3.59−3.82 (m, 4H, CH$_2$), 4.16−4.20 (m, 1H, CH), 7.41−7.48 (m, 6H, pyH, phH), 7.75−7.78 (m, 2H, pyH), 7.93−7.96 (d, 2H, pyH), 8.61−8.63 (d, 2H, pyH).

In a second step, a mixture of 0.5 g (0.0013 mol) of **1a** and 2 g of ammonium acetate were heated at 135 °C for 4 h. The dark reaction mixture was diluted with water, and the solid precipitate was filtered off, washed with water, dried, and recrystallized from 2-propanol and hexane, yielding 0.37 g of a crude product. Further purification was performed by column chromatography on silica gel first using toluene as an eluent and using then a 10:1 mixture of toluene and methanol. Yield: 0.13 g (26.5%). mp 122−125 °C. Elemental analysis, found: C, 69.98; H, 3.70; N, 11.18. Calcd for C$_{22}$H$_{14}$F$_3$N$_3$: C, 70.02; H, 3.74; N, 11.13. ^{1}H NMR (DMSO-d_6, 300 MHz) δ (ppm): 7.50−7.54 (m, 2H, pyH), 7.89−7.92 (d, 2H, phH), 8.00−8.05 (m, 2H, pyH), 8.10−8.13 (d, 2H, phH), 8.63−8.66 (d, 2H, pyH), 8.70 (s, 2H, pyH), 8.75−8.77 (d, 2H, pyH).

4′-[4-(1,4,7,10-Tetraoxa-13-azacyclopentadec-13-yl)]-2,2′:6′,2′′-terpyridine (bpb-A15C5, 5). A 0.4 g sample of powdered sodium hydroxide was added to a solution of 0.48 g (0.004 mol) of 2-acetylpyridine and 0.646 g (0.002 mol) of 4-(1,4,7,10-tetraoxa-13-azacyclopentadec-13-yl)benzaldehyde dissolved in 10 mL of ethanol. The reaction mixture was stirred for 24 h at room temperature and then poured into 200 mL of water. The yellow solid product was filtered off and purified by column chromatography on silica gel first using CHCl$_3$ and then using a 25:1 mixture of CHCl$_3$ and CH$_3$OH. The resulting diketone, a dark yellow oil, was used for the preparation of **5** without analysis.

A mixture of 0.4 g of the diketone and 3 g of ammonium acetate was heated at 150 °C for 3 h. The resulting dark oil was treated with water and then dissolved in 6 mL of acetonitrile. For the purification of the reaction product, 0.55 g of this compound was dissolved in 2 mL of ethyl acetate and filtered. A 3 mL volume of hexane was added to the filtrate, and the precipitate was filtered off after 5 h and washed with hexane. Yield: 10%. mp 112−115 °C. ^{1}H NMR (CDCl$_3$, 300 MHz) δ (ppm): 3.41−3.80 (m, 20H, OCH$_2$, NCH$_2$), 6.80−6.81 (d, $J = 8.8$ Hz, 2H, phH), 7.29−7.30 (m, 2H, pyH), 7.80−7.84 (m, 2H, pyH), 7.86−7.88 (d, $J = 8.5$ Hz, 2H, phH), 8.65−8.66 (d, $J = 8.1$ Hz, 2H, pyH), 8.75 (s, 2H, pyH), 8.76−8.77 (m, 2H, pyH).
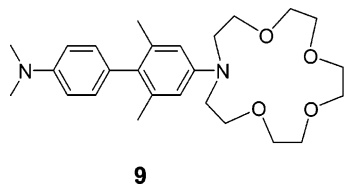
3. Results and Discussion

3.1. Absorption and Fluorescence Spectroscopy of Neutral bpb-R. *Steady-State Spectra and Solvatochromism.* For a better

SCHEME 2: Chemical Structures of Related D−A Biphenyls 6 and 6a and 4′-Aryl-Substituted Pyridines 7 and 8 with R = H, OMe, and DMA
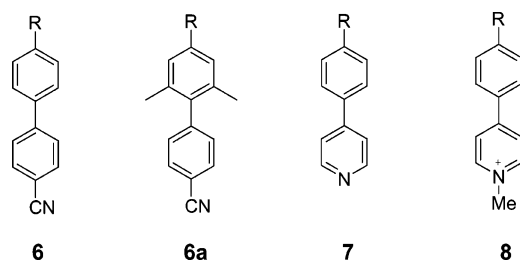
SCHEME 3: Chemical Structure of Related Bifunctional D−D Biphenyl Sensor Molecule 9

understanding of the underlying photophysics of the bpb-R series shown in Scheme 1 and the comparison to related D−A and D−D biphenyls depicted in Schemes 2 and 3, we investigated the spectroscopic properties of uncomplexed bpb-R in the aprotic solvents cyclohexane (CH), dibutyl ether (BOB), diethyl ether (Et$_2$O), chloroform, tetrahydrofuran (THF), dichloromethane, and acetonitrile (ACN) as well as in the protic solvents butanol (BuOH), ethanol (EtOH), and methanol (MeOH) prior to the protonation studies and to the complexation experiments introduced in part 2 of this series.[48] The absorption and fluorescence spectra of **1**−**5** in solvents of different polarities are illustrated in Figure 1 and also for **3** and **4** in the Supporting Information, and selected spectroscopic data are collected in Table 1. Some of the absorption and emission features of **2**, **3**, and **4** have been recently reported by Araki[62] as well as by Williams[64] and are taken into account in the discussion. As follows from Figure 1 and Table 1, the absorption spectra of bpb-R substituted with the weak acceptor CF$_3$ and the weak and medium donors H and OMe are only very slightly affected by solvent polarity. In contrast, the lowest energy absorption bands of bpb-DMA and bpb-A15C5 are bathochromically shifted with increasing solvent polarity. According to a comparison with the absorption spectra of the plain acceptor module terpyridine in cyclohexane and acetonitrile, the optical transitions at wavelengths below ca. 280 nm are ascribed to terpyridine-localized transitions. **1** and **2** display structured emission spectra in all the solvents used. In the case of **3**, structured emission spectra result only in solvents of low polarity such as cyclohexane, diethyl ether, BOB, and THF, with the vibronic structure vanishing almost completely in chloroform and dichloromethane (see the Supporting Information). Solvents of higher polarity starting from butanol yield broad and unstructured emission spectra that are red shifted and broadened with increasing solvent polarity. The spectroscopically very similar probes **4** and **5** carrying strong nitrogen donors show slightly structured emission spectra only in apolar cyclohexane. In all other solvents, they display broad and structureless emission spectra with the spectral position and width of the emission band depending on the solvent polarity (see the Supporting Information). Measurement of the excitation spectra of bpb-R at different emission wavelengths within the respective emission bands always yields matching spectra that strongly resemble the corresponding absorption spectra. The only exception here is **4** in methanol,
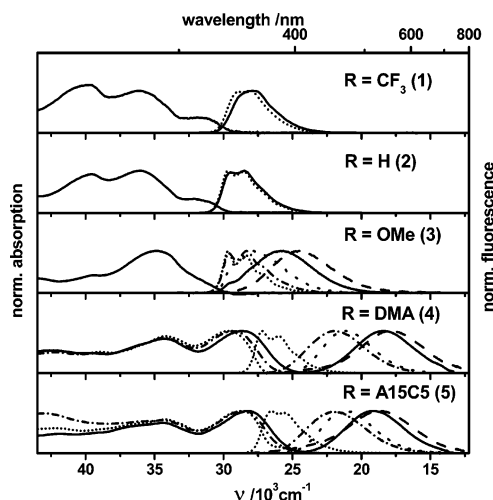

Figure 1. Normalized steady-state absorption spectra (left) and emission spectra (right) of bpb-R (compounds **1**−**5** from top to bottom; see Scheme 1) in MeOH (dashed line), CH$_3$CN (solid line), CH$_2$Cl$_2$ (dotted line), Et$_2$O (dash−dotted line), and cyclohexane (short dotted line). In the case of rather similar spectra, only spectra with sufficient deviations are depicted. The ligand concentration was 2×10^{-6} M in all cases. Excitation was at the longest wavelength absorption band.

where the excitation spectrum detected at ca. 420 nm differs slightly from the excitation spectra obtained at 500, 550, and 600 nm, respectively, which all match the ligand's absorption spectrum. The shoulder at 420 nm in the emission spectrum of **4** revealed in Figure 1 and in the Supporting Information is thus ascribed to traces of an emissive impurity that can be detected only under conditions where **4** is very weakly emissive. For all other solvents, this impurity could not be observed. Accordingly, for bpb-R, excitation of the lowest energy absorption band leads to the emitting state.

The intramolecular charge transfer character of **3**, **4**, and **5** is also reflected by an increase in the Stokes shift with increasing solvent polarity pointing to a stronger stabilization of the excited state in polar solvents. Consequently, for these molecules, excitation of the CT state involves a charge shift from the R-phenyl fragment to the terpyridine acceptor moiety with the dipole moment of the resultant excited state (μ_{es}) exceeding that of the respective ground state ($\mu_{es} > \mu_{gs}$). Terpyridine-localized transitions that typically include a charge transfer from the α-pyridine rings to the central pyridine group show only a very small solvent dependence. The excitation-induced change in dipole moment shown in Table 2 was determined according to the Lippert−Mataga formalism, i.e., from a plot of the Stokes shift ($\Delta\nu_{St}$) as a function of the solvent polarity parameter Δf displayed in Figure 2.[65−67] The slope of this plot reflects the increase in donor strength from R = CF$_3$ and H via OMe to DMA and A15C5 with $\Delta\nu_{St}$ being almost insensitive to solvent polarity for **1** and **2**, whereas a much steeper line and thus larger difference between the excited-state dipole moment and ground-state dipole moment, $\Delta\mu$, results for **3** and especially for **4** and **5**. From these solvatochromic plots, $\Delta\mu$ is calculated to 2.8, 2.4, 13.1, 18.4, and 20.7 D for **1**, **2**, **3**, **4**, and **5**, respectively; see Table 2. The values obtained for the latter three molecules underline the CT nature of the respective excited states. Our results are in reasonably good agreement with the values of μ_{es} of 2.1, 10.4, and 15.2 determined by Araki for **2**, **3**, and **4**[62] and are comparable in size to those reported for other D−A biphenyls such as **6** and **6a** (R = DMA).[36]

Fluorescence Quantum Yields and Solvatokinetics. As follows from Table 1 as well as from Figure 3, a reduction in solvent

TABLE 1: Spectroscopic Data of bpb-R in Different Solvents at 298 K

bpb-R	solvent	$\nu_{abs}{}^a \times 10^3/cm^{-1}$	$\nu_{em}{}^b \times 10^3/cm^{-1}$	fwhm$^c \times 10^3/cm^{-1}$	$\Delta\nu_{St}{}^d \times 10^3/cm^{-1}$	$\phi_f{}^e$
CF$_3$	CH	39.6, 36.0, 31.8	29.0, 28.2 (sh)	3.1	2.8	0.33
	Et$_2$O	39.7, 36.0, 31.8	28.9, 28.0 (sh)	3.2	2.9	0.26
	CH$_2$Cl$_2$	39.4, 35.9, 31.8	27.8	3.2	4.0	0.29
	CH$_3$CN	39.7, 36.1, 31.8	27.8	3.2	4.0	0.24
	MeOH	40.1, 36.0, 32.3	28.0	3.2	4.3	0.20
H	CH	39.5, 36.2, 32.6	29.6, 28.5 (sh)^f	3.2	3.0	0.26
	BOB	39.5, 36.1, 32.3	29.6, 28.5 (sh)	3.2	2.7	0.21
	CHCl$_3$	39.5, 35.9, 32.2	29.4, 28.2 (sh)	3.2	2.8	0.25
	Et$_2$O	39.6, 36.2, 32.2	29.6, 28.5 (sh)	3.2	2.6	0.18
	THF	39.4, 36.2, 32.2	29.4, 28.4 (sh)	3.2	2.8	0.17
	CH$_2$Cl$_2$	39.4, 36.1, 32.2	29.4, 28.2 (sh)	3.2	2.8	0.23
	BuOH	39.4, 35.8, 32.2	29.4, 28.6 (sh)	3.3	2.8	0.17
	CH$_3$CN	39.6, 36.2, 32.2	29.2, 28.4 (sh)	3.3	3.0	0.14
	EtOH	39.7, 36.0, 32.2	29.3 (sh), 28.5	3.2	3.7	0.15
	MeOH	39.9, 36.2, 32.2	29.3 (sh), 28.5	3.2	3.7	0.14
OMe	CH	35.0, 32.2 (sh)	29.7, 28.3 (sh)^f	3.1	2.5	0.23
	BOB	34.9, 32.2 (sh)	29.6, 28.3 (sh)^f	3.3	2.6	0.17
	CHCl$_3$	34.8, 32.2 (sh)	29.2 (sh), 27.9	3.8	4.3	0.19
	Et$_2$O	35.1, 32.2 (sh)	29.5 (sh), 28.3^f	3.5	3.9	0.16
	THF	34.8, 32.2 (sh)	29.4 (sh), 28.1	4.0	4.1	0.18
	CH$_2$Cl$_2$	34.9, 32.2 (sh)	29.1 (sh), 27.9	4.3	4.3	0.20
	BuOH	34.5, 32.2 (sh)	26.0	4.7	6.2	0.15
	CH$_3$CN	35.1, 32.2 (sh)	26.0	5.2	6.2	0.17
	EtOH	35.1, 32.2 (sh)	25.3	4.8	6.9	0.17
	MeOH	35.0, 32.2 (sh)	24.9	5.2	7.3	0.05
DMA	CH	34.4, 29.9	27.2, 26.2 (sh)	2.9	2.7	0.46
	BOB	34.5, 29.6	25.0	3.6	4.6	0.31
	CHCl$_3$	34.2, 29.0	22.9	3.7	6.1	0.24
	Et$_2$O	34.6, 29.7	22.7	4.7	7.0	0.22
	THF	34.2, 28.9	22.0	4.4	6.9	0.28
	CH$_2$Cl$_2$	34.3, 28.5	21.8	4.2	6.7	0.32
	BuOH	34.2, 28.6	19.2	5.0	9.4	0.03
	CH$_3$CN	34.4, 29.2	19.4	4.9	9.8	0.15
	EtOH	34.2, 28.8	19.5	5.0	9.3	0.01
	MeOH	34.6, 28.6	18.8	5.3	9.8	2×10^{-3}
A15C5	CH	34.3, 28.9	26.6, 25.7 (sh)	3.1	2.3	0.42
	BOB	34.2, 28.7	24.8	3.6	3.9	0.29
	CHCl$_3$	35.3, 28.6	22.5	4.0	6.1	0.27
	Et$_2$O	35.2, 28.7	22.8	4.7	5.9	0.26
	THF	35.8, 28.2	22.4	4.3	5.8	0.31
	CH$_2$Cl$_2$	35.8, 28.5	21.7	4.2	6.8	0.31
	BuOH	34.1, 27.8	19.6	4.7	8.2	0.06
	CH$_3$CN	36.0, 28.6	19.9	4.8	8.7	0.18
	EtOH	35.7, 28.3	19.8	4.6	8.5	0.03
	MeOH	35.6, 28.4	19.8	4.8	8.6	4×10^{-3}

^{a} Absorption maxima. ^{b} Emission maximum. ^{c} Emission bandwidth, i.e., full width at half-height of the maximum. ^{d} Stokes shift, i.e., energetic difference between the longest wavelength absorption band (or shoulder) and the emission maximum. ^{e} Fluorescence quantum yield. ^{f} Only two bands are given.

TABLE 2: Dipole Moments of bpb-R Derived from Solvatochromic Measurements

bpb-R	slope^a/cm^{-1}	a^b/Å	$\Delta\mu = \mu_{es} - \mu_{gs}$/D	$\mu_{gs}{}^c$/D	$\mu_{es}{}^d$/D
CF$_3$	527	5.3	2.8		
H	459	5.1	2.4	0.79	3.19
OMe	12 139	5.2	13.1	1.34	14.40
DMA	23 177	5.3	18.4	1.30	19.70
A15C5	19 630	6.0	20.7		

^{a} Slope of solvatochromic plot. ^{b} Onsager radius. ^{c} Ground-state dipole moment calculated for optimized ground-state geometry by AM1. ^{d} Excited-state dipole moment calculated using the Lippert equation $\Delta\nu_{st} = (2\Delta\mu^2/hca^3)\Delta f + $ constant, where $\Delta f = (\epsilon - 1)/(2\epsilon + 1) - (n^2 - 1)/(2n^2 + 1)$. The Onsager radius was derived using the mass−density formula $a = (3M/4\pi N_A\rho)^{1/3}$ and assuming $\rho = 0.95$ g/cm^3 for all compounds, with h and c having their usual meaning.

polarity enhances the fluorescence quantum yield of bpb-R. The strongest changes occur for **4** and **5** followed by **3**, whereas for **1** and **2** the effects are moderate. The lines in Figure 3—though only guides for the eye—reveal this trend of the solvent polarity dependence of the fluorescence quantum yields of the bpb-R series that can be categorized into the so-called positive solvatokinetic behavior with a decrease in emission yield with increasing solvent polarity. This suggests enhanced excited-state population of a highly polar charge transfer species with strongly nonradiative properties in highly polar solvents. These findings correlate with the tendency of the solvent dependence of the fluorescence quantum yield of **4** reported by Williams, although the actual values occasionally differ.[64] The comparatively low fluorescence quantum yields of **4** and **5** in the polar protic solvents butanol, ethanol, and methanol (see Table 1) indicate hydrogen bond induced or proticity quenching of fluorescence.
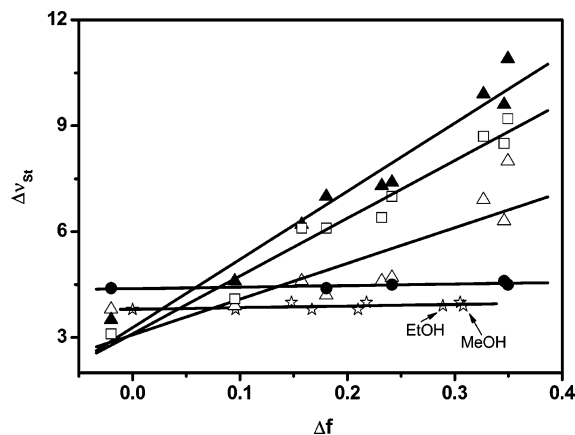
Bifunctional CT-Operated Fluorescent Probes. 1

J. Phys. Chem. A, Vol. 110, No. 38, 2006 **10961**

Figure 2. Stokes shift $\Delta\nu_{St}$ of bpb-R as function of solvent polarity with R = CF$_3$ (filled circle), H (star), OMe (open triangle), DMA (filled triangle), and A15C5 (open square).
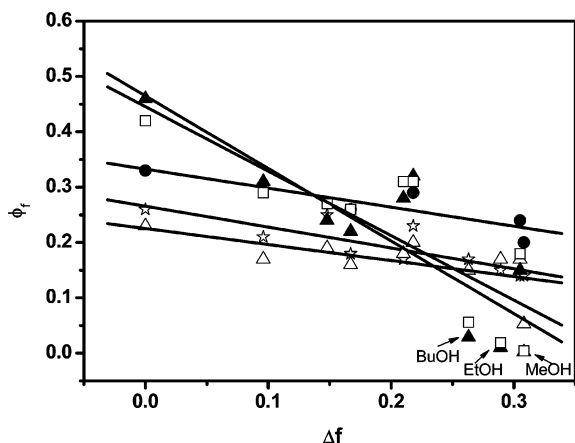

Figure 3. Fluorescence quantum yield of bpb-R as function of solvent polarity with R = CF$_3$ (filled circle), H (star), OMe (open triangle), DMA (filled triangle), and A15C5 (open square). The lines are only guides for the eye.

A similar behavior has been observed for other CT-operated fluorescent probes and has been also noticed, e.g., for pretwisted (sterically hindered) D−A biphenyl **6a** (Scheme 2).[36,68] This can be, for instance, employed to sensitively probe the proticity of organic solvents via hydrogen bond formation, as has been demonstrated for the latter molecule.[68]

Fluorescence Lifetimes, Radiative Rate Constants, and Nonradiative Rate Constants. To gain further insight into the excited-state processes involved in the relaxation of the fluorescence of bpb-R, the fluorescence decay kinetics were determined at several emission wavelengths within the respective emission bands. Time-resolved fluorescence measurements reveal monoexponential decay kinetics of bpb-R in all cases with the corresponding lifetimes being summarized in Table 3. The lifetimes of **4** measured by us in cyclohexane and THF are in excellent agreement with the data reported by Williams.[64] As follows from Table 3, the radiative and nonradiative rate constants k_f and k_{nr} that were calculated from the measured fluorescence quantum yields and lifetimes are barely affected by solvent polarity for **1**−**3** similar to what is observed for neutral biphenyls **6**.[36] However, the k_f values of **4** and **5** considerably depend on solvent polarity as revealed by a decrease of k_f from ca. 26×10^7 s^{-1} in cyclohexane to 3×10^7 s^{-1} in acetonitrile for both molecules; see Table 3 and Figure 4 exemplary for **4**. The most intriguing observation, however, is the atypical reduction in k_{nr} for **4** and **5** in polar solvents as compared to apolar ones.

3.2. Electronic Transitions in Neutral bpb-R. Quantum-chemical calculations have been performed representatively for **2** and **4** to obtain a more thorough understanding of the electronic states involved in the absorption and emission of bpb-R. The results are summarized in Table 4. As shown in Table 4, in the relatively large π-system of bpb-R, the absorption and fluorescence transition dipole moment can be oriented either along the biphenyl-type axis including the substituent R (*x*-axis) or perpendicular to it. In the latter case, the terpyridine system alone is involved yielding a so-called locally excited (LE) or terpyridine-localized transition, the properties of which should not depend or only weakly depend on the donor properties of the substituent R. On the other hand, the biphenyl-type transition should be strongly affected by the donor strength of R, resulting in a change of the energetics of the lowest excited state.

Based on semiempirical molecular orbital (MO) calculations (MOPAC/AM1), Araki[62] ascribed the lowest energy transition of **2** to a terpyridine (tpy) type $\pi_{tpy}-\pi^*_{tpy}$ (LE) transition because HOMO1, HOMO, and LUMO are mainly localized on the phenyl (π_{ph}), tpy (π_{tpy}), and tpy (π^*_{tpy}) moieties, and S$_1$ corresponds to the HOMO−LUMO transition. On the other hand, incorporation of a strong electron donor like DMA turns π_{ph} into the HOMO with the lowest energy transition now being of CT or $\pi_{ph}-\pi^*_{tpy}$ type. Our calculations that are similarly based on AM1 reveal that the longest wavelength transitions of **2** and **4** are allowed as follows from the high values of the oscillator strengths *f* and are both polarized in the *x*-direction (see Table 4). The energy difference between S$_1$ and S$_2$ is rather small, however. Table 4 also illustrates that the energy of the LE transitions of bpb-R, polarized in the *y*-direction, are only to a very small extent affected by the substituent R, whereas the CT transition, polarized along *x*, is strongly red shifted for strong donors R in accordance with the results from the spectroscopic studies revealed in the previous sections. The direction of the transition moment changes between S$_1$ (biphenyl axis along *x*) and S$_2$ (along the terpyridine *y*-axis). According to our calculations, nπ^* transitions are not found among the lowest excited states.

3.3. Protonation and Alkylation Studies with bpb-R: Spectroscopic Properties of Charged bpb-R. Protonation studies with bpb-R are performed (i) to establish their ability to serve as ratiometric fluorescent probes and to reveal substitution pattern, i.e., substituents of suitable D−A strength that yield fluorescent acceptor chelates and (ii) to conceive their potential as multimodal fluorescent sensors. The latter focuses on bifunctional **4** and **5**, which are designed for consecutive signaling of acceptor and donor protonation and are expected to exist in three spectroscopically distinguishable states: *neutral* (equaling no input), *A-protonated* (equaling the input *little protons*), and *A- and D-protonated* (equaling the input *many protons*). The results of these protonation studies provide the basis for the cation coordination experiments with bpb-R detailed in part 2 of this series[48] and the rational tuning of the fluorescence properties and analyte selectivity of this class of molecules by modulation of the acceptor strength of the A-receptor.[69] Accordingly, protonation-induced spectral and intensity changes in absorption and fluorescence are determined as a function of proton concentration and are compared within the bpb-R series. We chose acetonitrile here as solvent and not a protic one such as water or mixtures of water with organic solvents used for many analytical applications of fluorescent sensors because we aimed at a comparison of the spectroscopic features of the protonated bpb-R species to those of other neutral

TABLE 3: Fluorescence Lifetimes, Radiative Rate Constants, and Nonradiative Rate Constants of bpb-R at 298 K

bpb-R	solvent	$\phi_f{}^a$	$\tau_f{}^b$/ns	$k_f{}^c$/10^7 s^{-1}	$k_{nr}{}^d$/10^7 s^{-1}
CF$_3$	CH	0.33	2.4	14	28
	ACN	0.24	2.1	11	36
H	CH	0.26	1.9	14	39
	ACN	0.14	1.2	12	72
OMe	CH	0.23	2.1	11	37
	ACN	0.17	2.1	8	40
DMA	CH	0.46	1.8	26	30
	BOB	0.31	2.1	15	33
	Et$_2$O	0.22	3.1	7	25
	THF	0.28	5.2	5	14
	ACN	0.15	5.4	3	16
A15C5	CH	0.42	1.7	25	34
	ACN	0.18	5.5	3	15

[a] Fluorescence quantum yield. [b] Fluorescence lifetime. [c] Radiative rate constant $k_f = \phi_f/\tau_f$. [d] Nonradiative rate constant $k_{nr} = (1 - \phi_f)/\tau_f$.
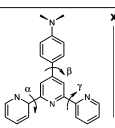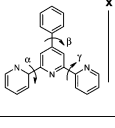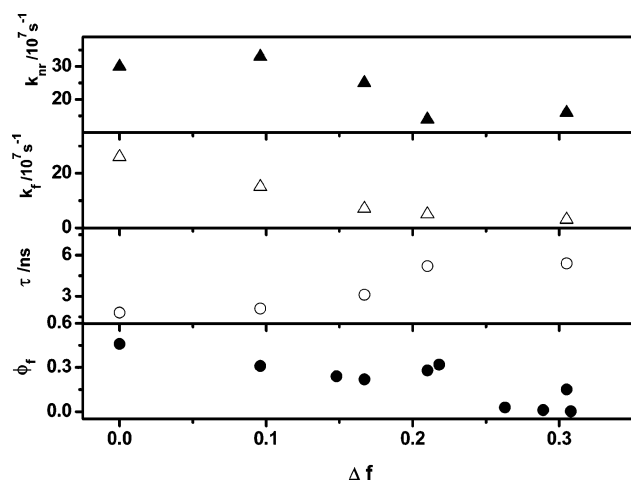

Figure 4. Fluorescence quantum yield (ϕ_f), fluorescence lifetime (τ), radiative rate constant (k_f), and nonradiative constant (k_{nr}) of **4** as function of solvent polarity.

TABLE 4: Transition Energies in eV, Oscillator Strengths f (in Parentheses), and Transition Polarization (See Axes) of 2 and 4 As Calculated by AM1 (CI = 10)^a

compound	S$_0 \rightarrow$ S$_1$	S$_0 \rightarrow$ S$_2$	S$_0 \rightarrow$ S$_3$	S$_0 \rightarrow$ S$_4$	S$_0 \rightarrow$ S$_5$
	4.06 (1.20)	4.65 (0.39)	4.90 (0.20)	4.97 (0.40)	5.34 (0.08)
	axis x	axis y	axis x	axis y	axis x
	4.65 (1.11)	4.74 (0.29)	4.84 (0.11)	5.06 (0.33)	5.27 (0.05)
	axis x	axis y	axis x	axis y	axis xy

[a] The x and y axes are in the plane of the molecules. The twist angles used for the calculation were those determined for the stable ground-state minimum.

and ionic D−A biphenyls (see Scheme 2) and a new D−D biphenyl sensor molecule **9** (see Scheme 3), all studied in acetonitrile.

Protonation of bpb-R is expected to occur first at the terpyridine moiety, thereby increasing the acceptor strength and transforming neutral bpb-R into a charged, i.e., ionic species. Furthermore, terpyridine protonation should be enhanced in the excited state due to an increase in basicity of the terpyridine nitrogen atoms upon charge transfer from the R-phenyl fragment toward terpyridine. Additionally, as terpyridine contains three
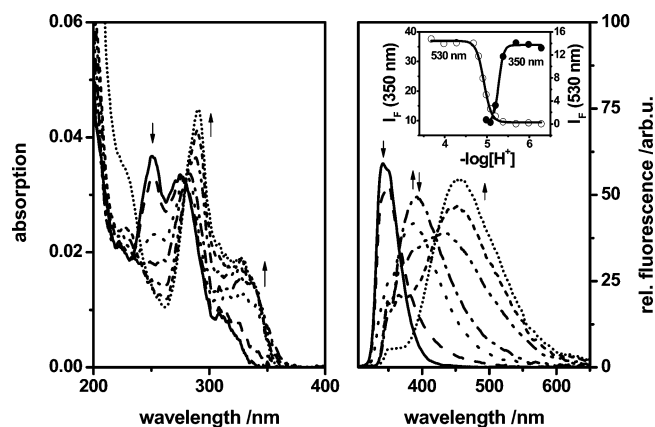

Figure 5. Effect of protonation on the absorption (left) and fluorescence (right) spectra of bpb-R with R = H (**2**) in ACN for selected proton-to-ligand concentration ratios: 0:1 (solid line), 4:1 (dashed line), 6:1 (dotted line), 8:1 (dash−dotted line), 12:1 (dash−dot−dotted line), 15:1 (short dashed line) and 200:1 (short dotted line). The probe concentration was 1×10^{-6} M; excitation was at 277 nm (isosbestic point). Inset (right): Fluorescence intensity as function of proton concentration determined at 350 and 530 nm, i.e., at the maximum of the emission bands of unprotonated and doubly protonated bpb-H.

potential protonation sites,[70] i.e., three nitrogen heteroatoms, multiple acceptor protonation is likely. Spectroscopically distinguishable monoprotonation and double protonation of terpyridine in water has been reported by Martin,[71] whereas Chakravorti[72] could detect only doubly protonated terpyridine. Also, for related 4′-(4-N,N-diphenylaminophenyl)-2,2′:6′,2″-terpyridine in ethanol, only the doubly protonated weakly emissive species could be obtained.[21] Triple protonation is very unlikely due to the increasingly positive charge of the protonated terpyridine fragment and the planar geometry of doubly protonated terpyridine.

Acceptor Protonation of 2 and 3. Protonation of the A-receptor terpyridine is expected to occur exclusively for the sensor molecules **2** and **3**. An example for a pH titration is shown in Figure 5 for **2**. As revealed by the red shift of the absorption and emission bands, terpyridine protonation results in the expected enhancement of the molecule's CT character.[73] In the case of the absorption spectra, not only the spectral position of the absorption bands changes successively with increasing proton concentration but also the shape of the bands and structure: the absorption bands of neutral **2** located at 250, 274, and 309 nm, respectively, vanish and new bands centered at 290 and 330 nm appear. The lowest energy absorption band that exclusively occurs for the protonated species is ascribed to a CT band involving a charge transfer from the R-phenyl fragment to the protonated terpyridine module, whereas the

TABLE 5: Effect of Protonation and Alkylation on the Spectroscopic Properties of bpb-R in ACN at 298 K

compound	$\nu_{abs}{}^a \times 10^3/cm^{-1}$	$\nu_{em}{}^b \times 10^3/cm^{-1}$	$\Delta\nu_{St}{}^c \times 10^3/cm^{-1}$	$\Delta\nu_{fp-cp}{}^d \times 10^3/cm^{-1}$	ϕ_f
1	31.8	27.8	4.0		0.24
1⊂H$^+$	30.2	25.6	4.6	1.7, 2.6	0.27
prot **1**	30.6	28.0	2.6	1.3, 0.2	0.69
2	32.2	29.2, 28.4 (sh)	3.0		0.14
2⊂H$^+$	30.6	25.5	5.1	1.9, 2.9	0.28
2⊂2H$^+$	30.8	22.0	8.8	1.7, 6.4	0.32
2⊂H$^+$,Me$^+$	30.8	22.3	8.5	1.5, 6.2	0.16
2⊂2Me$^+$	30.8	22.0	8.8	1.5, 6.5	0.08
3	35.1, 32.2 (sh)	26.0	6.2		0.17
3⊂H$^+$	29.7	20.2	9.5	1.9, 5.8	0.07
3⊂2H$^+$	31.5	17.0	14.5	0.1, 9.0	4×10^{-3}
4	29.2	19.4	9.8		0.15
4⊂*x*H$^+$	21.4	n.d.	n.d.	7.5, n.d.^{e}	n.d.
H$^+$⊃**4**⊂*x*H$^+$	30.3	28.1	2.2	−1.4, −9.3	0.43

^{a} Lowest energy absorption band. ^{b} Emission maximum. ^{c} Stokes shift. ^{d} Analyte-induced spectral shift in absorption (first value) and emission (second value) between free probe and protonated or alkylated probe with "fp" and "cp" equaling free probe and coordinated probe. ^{e} n.d., not determined.

energetically higher lying optical transitions are attributed to terpyridine-localized transitions. As expected for the chosen design concept, the size of the protonation-induced effects in emission considerably exceeds that in absorption. Successive addition of protons to **2** leads to the consecutive appearance of two species displaying emission bands of CT nature that differ considerably in spectral position and only slightly in fluorescence quantum yield. Up to a proton-to-ligand concentration ratio of ca. 8:1, single protonation of the terpyridine acceptor occurs as communicated by a newly formed emission band at 391 nm. A further increase in proton concentration is accompanied by the decrease of this emission band and the appearance of another emission band centered at 454 nm. The influence of proton concentration on the fluorescence intensities measured at 350 nm, i.e., at the maximum of the ligand's emission band, and at 530 nm within the emission band of completely protonated **2**, respectively, is illustrated in the inset of Figure 5. The sigmoidal shape of both plots is typical for such a type of titration. No attempts are made by us to determine the corresponding protonation constants as the pH titrations suggest high protonation constants, the measurement of which is rather erroneous with optical methods.

The straightforward course of terpyridine protonation is revealed by an isosbestic point at 277 nm and two isoemissive points at 366 and 425 nm (see Figure 5). The former isoemissive point is observed for proton-to-ligand concentration ratios of 0:1 to 8:1, and the latter is observed from 8:1 to 200:1. The intriguingly strong changes in emission indicate consecutive monoprotonation and double protonation of **2** yielding A-monoprotonated and A-doubly protonated **2**, i.e., **2**⊂H$^+$ and **2**⊂2H$^+$. The protonation-induced changes can be reversed upon addition of base, e.g., triethylamine. With values of 0.28 and 0.32, the fluorescence quantum yields of **2**⊂H$^+$ and **2**⊂2H$^+$ are astonishingly high and exceed the fluorescence quantum yield of **2** by a factor of ca. 2; see Table 5, which summarizes the spectroscopic data of neutral and protonated bpb-R.

Protonation of the terpyridine moiety of **3** similarly yields red shifts in absorption and emission; see Table 5 and Figure 6, which compares the protonation-induced spectroscopic effects within the bpb-R family. The emission spectra in Figure 6 are weighted by fluorescence quantum yield to illustrate the protonation-induced modulations in fluorescence intensity. Protonation of **3** also occurs consecutively and straightforwardly as indicated by isosbestic points at 303 nm (**3** → **3**⊂H$^+$; absorption bands at 285 and 317 nm for **3** and at 290 and 334 nm for **3**⊂H$^+$) and at 300 and 331 nm (**3**⊂H$^+$ → **3**⊂2H$^+$; 290
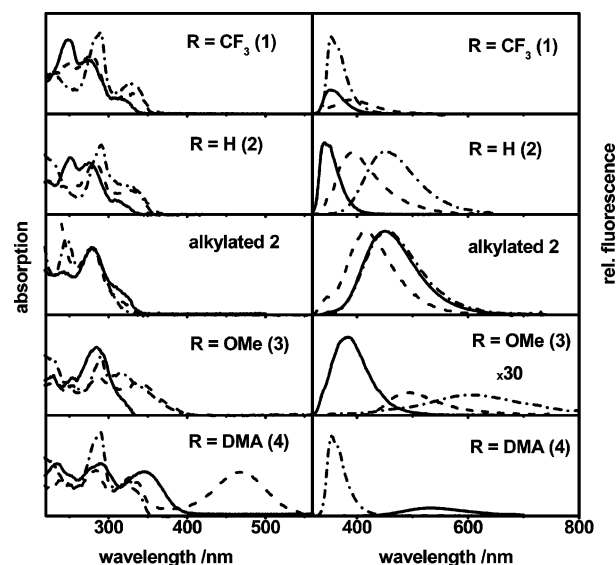

Figure 6. Effect of protonation on the absorption (left) and quantum yield weighted emission (right) of bpb-R in ACN: unprotonated (solid line), monoprotonated (dashed line), and completely protonated probe (dash−dotted line). The monoprotonated species of bpb-DMA is nonemissive. Weighting of the emission spectra of **1**−**5** with the respective relative fluorescence quantum yields was performed for each substituent R individually with the quantum yield of the free ligand equaling 1. The emission spectrum of doubly protonated bpb-OMe is multiplied by a factor of 30 for better visualization. For comparison, the normalized absorption and normalized emission spectra of monoalkylated and doubly alkylated bpb-H (**2**), i.e., the model systems bpb-H⊂H$^+$,Me$^+$ **10** (solid line) and bpb-H⊂2Me$^+$ **11** (dash−dotted line), shown in Scheme 4, are included as well as deprotonated bpb-H⊂H$^+$,-Me$^+$ (dashed line) obtained upon addition of triethylamine to bpb-H⊂H$^+$,Me$^+$. The ligand concentration was 2×10^{-6} M in all cases. Excitation was at the longest wavelength absorption band.

and 317 nm for **3**⊂2H$^+$), respectively. Similarly to **2**, two distinct and strongly red shifted emission bands at 495 nm (**3**⊂H$^+$) and 621 nm (**3**⊂2H$^+$) are observed that indicate successive acceptor protonation. The enhanced D−A strength of **3** as compared to **2** is revealed by the size of the protonation-induced spectral shifts in absorption and especially in emission, summarized in Table 5 and Figure 6. The fluorescence quantum yield of monoprotonated **3** is reduced by a factor of ca. 2 in comparison to the parent probe, and doubly protonated **3** is only weakly emissive.

Acceptor and Donor Protonation of Bifunctional 4. As follows from Table 5 and Figure 6 as well as from Figure 7
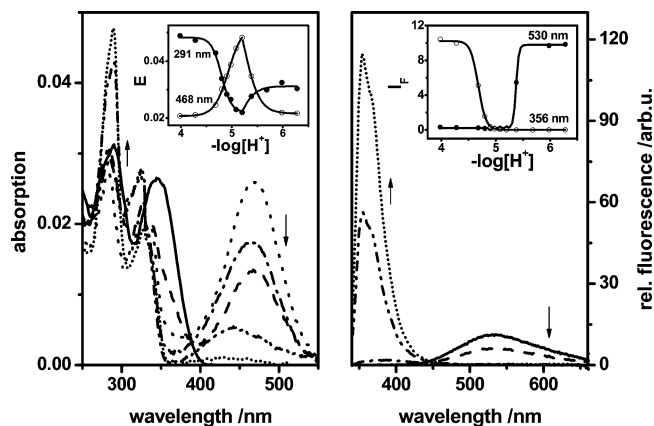
Figure 7. Effect of protonation on the absorption (left) and emission (right) spectra of bpb-R with R = DMA (**4**). Selected proton-to-probe concentration ratios: 0:1 (solid line), 4:1 (dashed line), 6:1 (dotted line), 10:1 (dash−dotted line), 20:1 (dash−dot−dotted line), and 100:1 (short dotted line). The probe concentration was 1×10^{-6} M, the solvent was ACN, and excitation was at 330 nm (isosbestic point). Inset: Absorbance (left) and fluorescence intensity (right) at selected wavelengths, i.e., absorption and emission maxima, as a function of proton concentration.

Figure 8. Comparison of the normalized emission spectra of bpb-R with R = H (**2**) (dashed line), monoprotonated bpb-H (open circles, 1:8), bpb-CF$_3$ (solid line), and completely protonated bpb-DMA (open triangles, 1:100). The ligand concentration was 2×10^{-6} M for all the systems studied. The proton-to-ligand concentration ratios used are given in the parentheses. Excitation was at the lowest energy absorption band.

depicting the absorption and fluorescence properties of the bifunctional probe **4** as a function of proton concentration, the trend of the spectroscopic effects accompanying the protonation of the A-receptor terpyridine are further enhanced for **4** as compared to **2** and **3** substituted with a weak and a medium-sized donor. Terpyridine protonation of **4** leads to the appearance of absorption bands at 284, 329, and 468 nm, with the latter clearly being of CT nature. The emission of monoprotonated **4** and that of doubly protonated **4** are completely quenched and/or red shifted to a wavelength region inaccessible to our fluorometer (>850 nm). Further addition of protons and thus eventually protonation of the DMA group, however, shifts the absorption and emission of A-protonated **4** ($\textbf{4} \subset x\text{H}^+$) strongly to the blue and switches its emission ON, i.e., transforms a more or less nonemissive species into a strongly emissive one with a fluorescence quantum yield of 0.43. This value is astonishingly high compared to the fluorescence quantum yields of 0.24 and 0.14 found for **1** and **2** (see Table 5). It is intriguing to note the strong resemblance between the absorption spectra of A- and D-protonated **4** ($\text{H}^+ \supset \textbf{4} \subset x\text{H}^+$) and $\textbf{2} \subset \text{H}^+$ (see Table 5 and Figure 6), as well as between $\text{H}^+ \supset \textbf{4} \subset x\text{H}^+$ and fully protonated **1**, the protonation behavior of which is discussed in the next subsection. The slightly structured emission spectrum of $\text{H}^+ \supset \textbf{4} \subset x\text{H}^+$ that reveals its weak D−A strength, however, resembles the emission spectrum of **2** and differs considerably from the emission spectrum of $\textbf{2} \subset \text{H}^+$; see also Figure 8 comparing the emission spectra of selected neutral and protonated bpb-R molecules. The weak CT character of completely protonated **4** may be ascribed to an inductive acceptor effect of the positively charged nitrogen of the DMA group. Similar protonation-induced effects are observed for **5** designed as a bifunctional cation sensor that are not detailed here.

Also in the case of **4** as well as **5**, protonation occurs straightforwardly and consecutively, here first at the terpyridine fragment and then at the less basic DMA group. To illustrate the advantages and analytical potential of such a bifunctional pH-responsive probe, protonation-induced changes in the absorption and fluorescence intensity of **4** at selected wavelengths, i.e., at the absorption and emission maxima of neutral **4** and its differently protonated analogues, are displayed in the inset of Figure 7. Intriguing are the proton concentration dependences
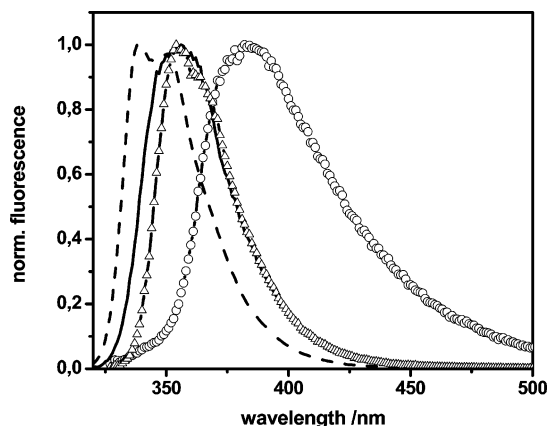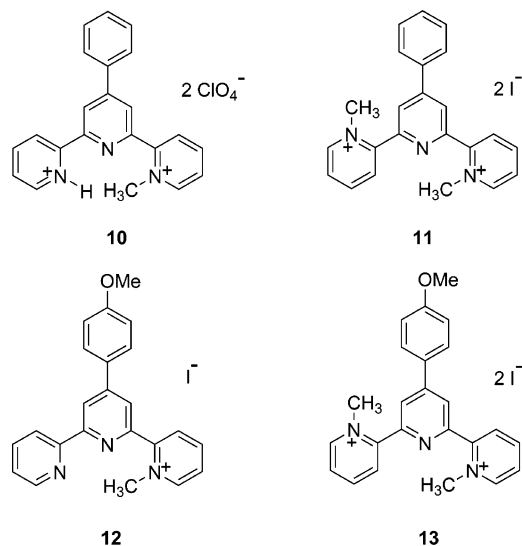
of the emission changes at 530 and 356 nm that can be combined for proton sensing over an extended dynamic range. The acidity constant for donor protonation of $\textbf{4} \subset x\text{H}^+$ is determined to 4.5 (log K_s) from absorption and emission measurements.

Protonation of 1. Astonishingly, protonation of **1** substituted with a weak CF$_3$ acceptor yields more complex effects; see Figures 6 and 8, Table 5, and the Supporting Information. The reversible protonation-induced bathochromic shifts in absorption and emission of **1** and the spectral position of the respective absorption and emission bands that resemble those of $\textbf{2} \subset \text{H}^+$ point to monoprotonation of the terpyridine acceptor as a first step. Interestingly, the emission maximum of monoprotonated **1** is slightly red shifted compared to that of $\textbf{2} \subset \text{H}^+$. However, the blue shift in emission resulting for completely protonated **1** (prot **1**) in combination with the high fluorescence quantum yield of 0.69 (see Table 5) is indicative of a weakening of the D−A strength as encountered for $\text{H}^+ \supset \textbf{4} \subset x\text{H}^+$. These spectroscopic data suggest an interaction between protons and the CF$_3$ group that is, however, chemically not very plausible. The exact nature of prot **1** is still not clear yet and is the object of ongoing research. The constant for complete protonation (log K_s) of **1** (formation of prot **1** from $\textbf{1} \subset \text{H}^+$; see Table 5) is determined to 5.1 and 5.2 from absorption and emission measurements, respectively.

Comparison of Protonated and Alkylated bpb-R. The astonishingly strong protonation-induced spectral changes in **2** and **3**, the clear spectroscopic distinction between the monoprotonated and doubly protonated species, and the comparatively high fluorescence quantum yields of the respective acceptor chelates encouraged us to synthesize bisalkylated **2**, i.e., $\textbf{2} \subset 2\text{Me}^+$ and its monoprotonated monoalkylated analogue $\textbf{2} \subset \text{H}^+,\text{Me}^+$, molecules **11** and **10** in Scheme 4. The goal here—representatively for **2**—was the identification of the actual protonation sites in bpb-R and the control of our species assignment by comparison of the spectroscopic properties of alkylated **2** to that of $\textbf{2} \subset 2\text{H}^+$. With X-ray analysis of $\textbf{2} \subset \text{H}^+,\text{Me}^+$ and $\textbf{2} \subset 2\text{Me}^+$, we determined the (solid state) alkylation and protonation sites in **2** to be the 2- and 6-pyridine groups, respectively.[63,74] The close resemblance between the absorption and emission spectra of $\textbf{2} \subset 2\text{Me}^+$, $\textbf{2} \subset \text{H}^+,\text{Me}^+$, and $\textbf{2} \subset 2\text{H}^+$ (see Figure 7 and Table 5) verifies our species assignment. Interestingly, in contrast to the close resemblance of their spectral features, the fluorescence quantum

Bifunctional CT-Operated Fluorescent Probes. 1

J. Phys. Chem. A, Vol. 110, No. 38, 2006 **10965**

SCHEME 4: Chemical Structures of Alkylated bpb-R 10−13

10

11

12

13

yields of $2 \subset H^+, Me^+$ and $2 \subset 2Me^+$ vary from that of $2 \subset 2H^+$ by a factor of 2 and 4, respectively.

Fluorescence Lifetimes and Radiative Rate Constants of Protonated and Alkylated bpb-R. To gain further insight into the excited-state processes involved in the relaxation of the fluorescence of protonated and alkylated bpb-R, we studied the fluorescence decay kinetics of these species at several emission wavelengths within the respective emission bands. In all cases, monoexponential decay kinetics were obtained. In Table 6, the corresponding lifetimes as well as the radiative and nonradiative rate constants are compared to those of the neutral sensor molecules. The most prominent features in Table 6 are (i) the protonation- or alkylation-induced decrease in k_f for **2** and **3** with k_f reaching similarly small values as observed for neutral, i.e., unprotonated, **4** and **5** in polar solvents (see also section 3.1 and Table 3), (ii) the high values of k_f resulting for $H^+ \supset 4 \subset xH^+$ and completely protonated **1**, and (iii) the protonation- and/or alkylation-induced changes in k_{nr}. For instance, for **2** substituted with a weak donor, k_{nr} is diminished by a factor of ca. 7 upon both monoprotonation and double protonation despite the considerably red shifted emission spectra of $2 \subset H^+$ and $2 \subset 2H^+$, whereas for medium-sized donors such as the methoxy group, the nonradiative rate constant is enhanced slightly by monoprotonation and strongly by double protonation.

3.4. Calculation and Comparison of the Ground and Excited Potentials of Neutral and Charged bpb-R. When comparing neutral and ionic biphenyls, it has been found that, for the ionic compounds, the ground-state barriers to rotation around the 90° twist angle are larger, the amount of CT character upon excitation of the planar molecule increases, and the shape of the potential energy changes and acquires a pronounced minimum at 90° in the excited state.[36,75,76] The missing activation barrier toward twisting in the excited state allows ionic biphenyls such as **8** to reach the perpendicular CT minimum, whereas their neutral counterparts with a weaker D−A character rather relax to a more planar excited-state conformation. Furthermore, the small fluorescence quantum yields suggest that a S_0/S_1 conical section not too far from the 90° minimum is accessible for the ionic biphenyls, probably due to the smaller S_0-S_1 energy gap.

For a deeper understanding of the spectroscopic features of neutral and charged, i.e., protonated or alkylated, bpb-R, we performed quantum-chemical calculations with the model py-

ridine molecules **14−16** and the model ionic pyridinium compounds **17−19** shown in Scheme 5. The ultimate goal here was to correlate the nonradiative decay rates and the trends observed for the fluorescence quantum yields of the neutral and ionic, i.e., protonated, bpb-R species with the size of the ground-state and excited-state barriers to rotation around the 90° twist angle.

The neutral model pyridines **14−16** behave very similarly to **6** and **6a**;[75] i.e., small barriers to rotation in the ground state occur around 0.07 eV for planarization and around 0.05 eV for reaching the 90° conformation. The minima are very shallow with values of ca. 0.07 eV and are situated at an angle of ca. 35−40°. In the excited, i.e., S_1, state, both barriers increase such that the most stable conformation is now found around 30°. The barrier height at 90° decreases from **14** to **16** with increasing donor strength of the substituent R. Due to the still significant size of the barrier at 90°, it is photophysically difficult to reach the twisted intramolecular charge transfer (TICT) conformation by S_1-state relaxation, although in a highly polar solvent, the TICT state with its very high dipole moment can be sufficiently stabilized to become populated as suggested, e.g., by the previously discussed polarity dependence of the radiative rate constants of bpb-R. The ground- and excited-state potentials are qualitatively different for the ionic model systems **17−19** as compared to the corresponding neutral compounds **14−16**. In the ground state, the barrier at 90° is much larger and increases significantly with the donor strength of R. In the excited state, however, the barrier at 90° completely vanishes such that this conformation becomes a stable minimum even in the gas phase, and there is no barrier to rotation and relaxation when the molecule reaches the Franck−Condon conformation through excitation from the ground state. There is a clear tendency for preferential stabilization of the excited-state perpendicular minimum with increasing donor strength of R, i.e., from **17** to **19**. Analysis of the electronic distribution indicates that the 90° conformation is characterized by a full electron transfer from the donor to the acceptor moiety across the twisted bond. These findings explain the very small k_f values found for acceptor-protonated or acceptor-alkylated bpb-R (see Table 6), and they reveal the forbidden nature of the emission from the perpendicular minimum with TICT character. Protonation of both the acceptor receptor and the donor receptor leads to a strong increase of k_f because this species does not relax to 90°, i.e., the perpendicular minimum disappears due to the strongly decreased D−A character. See also the discussion in the next section.

**3.5. Spectroscopic Features of Neutral and Charged bpb-R within the Framework of Neutral and Ionic D−A Biphenyls.** For a better understanding of the spectroscopic features of neutral and charged, i.e., protonated and alkylated, bpb-R and to conceive structure−property relationships for biphenyl-type molecules that form at least moderately emissive acceptor chelates in highly polar solvents, we compare the spectroscopic properties of neutral, A-coordinated, and A- and D-coordinated bpb-R exemplary to those of neutral and ionic biphenyls **6, 6a, 7**, and **8** depicted in Scheme 2. For these D−A biphenyls substituted with sufficiently strong D−A substituents, the spectral positions of the absorption and emission bands are shifted to the red with increasing D−A strength in polar solvents due to the admixture of polar resonance structures. In the majority of cases, simultaneously both the radiative rate constants and fluorescence quantum yields strongly decrease.[36,37,68] Calculations[36,75] indicate that this behavior can be ascribed to a solvent polarity-induced deformation of the excited-

TABLE 6: Fluorescence Lifetimes, Radiative Rate Constants, and Nonradiative Rate Constants of Protonated and Alkylated bpb-R in ACN

compound	$\phi_f{}^a$	$\tau_f{}^b$/ns	$k_f{}^c$/10^7 s^{-1}	$k_{nr}{}^d$/10^7 s^{-1}
1	0.24	2.1	11	36
1⊂H$^+$	0.27	2.5	11	29
prot **1**	0.69	2.7	26	11
2	0.14	1.2	12	72
2⊂H$^+$	0.28	7.0	4	10
2⊂2H$^+$	0.32	7.4	4	9
2⊂H$^+$,Me$^+$	0.16	6.9	2	12
2⊂2Me$^+$	0.08	4.8	2	19
3	0.17	2.1	8	40
3⊂H$^+$	0.07	1.8	4	52
3⊂2H$^+$	4×10^{-3}	0.3	1	332
4	0.15	5.6	3	15
H$^+$⊃**4**⊂xH$^+$	0.43	1.9	23	30

^{a} Fluorescence quantum yield. ^{b} Fluorescence lifetime. ^{c} Radiative rate constant $k_f = \phi_f/\tau_f$. ^{d} Nonradiative rate constant $k_{nr} = (1 - \phi_f)/\tau_f$.

SCHEME 5: Pyridine Systems 14−16 and Pyridinium Systems 17−19 Used as Model Compounds for Neutral and Charged, i.e., Protonated or Alkylated, bpb-H, bpb-OMe, and bpb-DMA for Quantum-Chemical Calculations

14 **15** **16** **17** **18** **19**
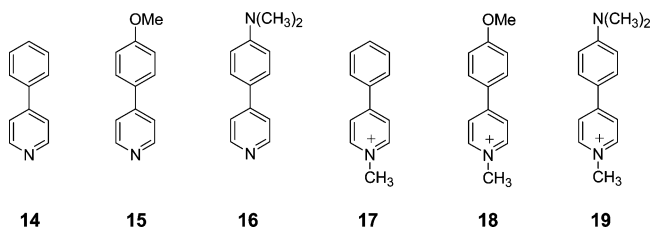
state rotational potential because the dipole moment of the perpendicular conformation exceeds that of the planar one, resulting in a stabilization of the perpendicular structure in polar solvents. This can lead to a complete change of the photophysical properties, if the polar solvent-induced potential deformation creates an energy minimum for the perpendicular conformation[77] that can be experimentally recognized by its forbidden emissive properties. For instance, sterically hindered **6a** populates an emissive TICT state in polar solvents.[36,37] If the cyanobenzene group is replaced by an even stronger acceptor, such as a charged pyridinium group in **8**, the excited-state potential is most likely deformed in such a way that the perpendicular conformation should present the energy minimum in all solvents.[77] Under these conditions, a strong nonradiative fluorescence deactivation pathway starts to be active, probably connected with a nearby conical intersection with the ground state. The photophysical properties of ionic or charged D−A biphenyl-type molecules that can freely rotate around the aryl−aryl bond are thus expected to reveal small radiative and large nonradiative rate constants and accordingly should be only very weakly emissive, at least when substituted with strong donors.[36,75]

Spectroscopic Features of Neutral bpb-R 1−5 within the Framework of Neutral D−A Biphenyls. As has been illustrated in section 3.1, the most remarkable spectroscopic features of neutral bpb-R are (i) red shifted absorption and emission bands for strong donors R and (ii) small k_f but also comparatively small k_{nr} values for **4** and **5** in highly polar solvents and accordingly still moderate fluorescence quantum yields. The photophysical properties of neutral bpb-R are mainly governed by structural changes of the twist angle in the excited state controlled by the molecule's D−A strength similarly to other D−A biphenyls; see also section 3.4.[36,75,77] As is to be expected, the terpyridine moiety present in the bpb-R molecules investigated here is a stronger acceptor than the cyanobenzene and the pyridine group of **6** and **7**. This follows, e.g., from a comparison of the spectral position of the emission maxima of
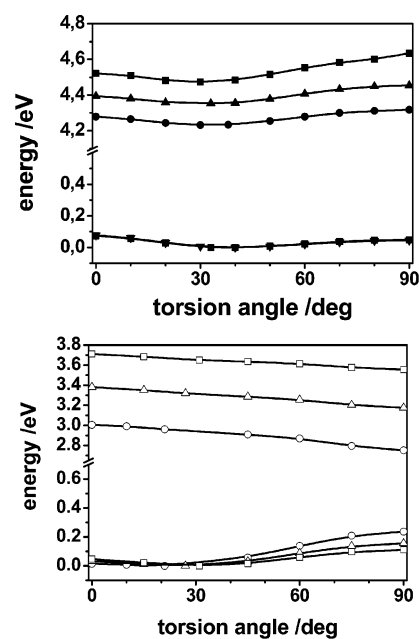
Figure 9. S$_0$ and S$_1$ potentials of the model pyridine compounds **14−16** (top, filled symbols) and model pyridinium compounds **17−19** (bottom, open symbols) calculated with AM1 (ground state) and AM1+Zindo/CI (excited state): **14** (filled square), **15** (filled triangle), **16** (filled circle), **17** (open square), **18** (open triangle), and **19** (open circle). The S$_0$ potentials of **14**, **15**, and **16** are nearly identical, and not all symbols are shown for clarity.

bpb-R, **6**, and **7** in highly polar solvents such as acetonitrile. Compared to pyridine, in terpyridine the electron density of the central pyridine ring is decreased by the electron-accepting 2- and 6-pyridine substituents. The higher acceptor strength of the terpyridine fragment on the whole leads to an increased electron density shift from the donor group. This can account for the hydrogen bonding-induced diminution in fluorescence quantum yields observed for **3** and especially for **4** and **5** in protic solvents (see Table 1). Similar effects occur, e.g., for pretwisted **6a**[36,68] as well as for D−A biphenyls substituted with a pyrimidine acceptor,[83] but not for **6**.[36]

The decrease in k_f for neutral bpb-R in the order **1** ∼ **2** < **3** < **4** ∼ **5** observed, e.g., in acetonitrile, that correlates with the molecule's D−A strength is understandable by comparison with other known D−A biphenyl systems such as dimethylamino cyano biphenyls **6** and **6a**. This effect is ascribed to conformational relaxation of the initially formed near-planar Franck−Condon (FC) CT state to an emissive CT state of twisted conformation with a perpendicular energy minimum and correspondingly low radiative rate constants in highly polar

solvents.[36,77] For this conformation, the radiative rate constants are small but nonzero due to a broad angular distribution around the energy minimum. In apolar solvents such as cyclohexane and in weakly polar solvents such as dibutyl ether, the energy minimum of the twisted CT state of **4** and **5** is higher in energy than the energy minimum of the (near) planar CT state and cannot be populated. Accordingly, comparatively high radiative rate constants are observed, revealing the allowed nature of the emissive conformation. This interpretation is supported by the resemblance between the spectral position of the emission bands and radiative rate constants of **4**, **5**, and pretwisted **6a**.[36] The medium-strong solvatochromism and the intermediate size of k_{f} of the methoxy derivative **3** suggest that, for this molecule, the main conformation of the emissive state is nearly planar, also in polar solvents. Prerequisite for moderately sized k_{f} values of bpb-R in polar solvents is a weak D–A character as conceived in **1** and **2**. For these molecules, the small solvent dependence of k_{f} in combination with the slightly structured emission spectra suggests fluorescence from a photochemically nonreactive state with weak CT and less forbidden properties in all the solvents investigated.

Whereas the size of the k_{f} values in Table 3 is a direct indication of the average conformation of the bpb-R molecules, i.e., twisted or nontwisted, the size and trends of the k_{nr} values within the bpb-R family are more difficult to interpret. It is remarkable that the nonradiative rates increase in highly polar solvents for **1** and especially for **2**, are sizable independent of solvent polarity in the case of medium-sized donors as found in **3**, and decrease by a factor of ca. 2 for **4** and **5** substituted with strong dialkylamino donors in polar as compared to apolar solvents. The latter behavior that is rarely observed for CT-operated fluorescent probes contradicts the energy gap rule that predicts an increase of k_{nr} with a narrowing of the S_1–S_0 energy gap.[78,79] This observation supports a change in the nature of the emissive state with solvent polarity for **4** and **5**. As follows from Tables 1 and 3, the reduction in k_{nr} accounts for the moderate drop in fluorescence quantum yield by a factor of only 3 occurring for both sensor molecules when switching from apolar cyclohexane to highly polar acetonitrile. This explanation resulting in a behavior opposing the usual energy gap rule, though plausible and tempting, is, however, only a qualitative one. It is derived from radiative and nonradiative rate constants as calculated from measured fluorescence quantum yields and fluorescence lifetimes and relies on the assumption that the yield of formation of the CT state is unity. This is fulfillled, at least for **4** and **5**, in solvents of medium and high polarity where no LE emission is observed. Within a general scenario where the initially excited LE state relaxes to an emissive CT state, the measured fluorescence quantum yield is in fact the product of the formation yield of the CT state and its fluorescence quantum yield. Except for the case where the yield of CT formation is 1, the true CT state radiative yield is thus larger than the one measured which accordingly affects the derived k_{f} and k_{nr}. However, the qualitative trends drawn from the data reported in section 3.1. are sufficient to deduce the desired structure–property relationship for D–A biphenyl-type sensor molecules; see also the forthcoming section on charged bpb-R. Accordingly, no attempts have been made, e.g., to determine radiative rate constants from absorption spectra to discriminate the emission from the initially excited state or from a transient state that could not be detected within the limited time resolution of our setup.

A behavior similar to that observed for **4** and **5** has been reported for **6a**,[36,37] where the sterical hindrance by two ortho methyl substituents leads to a strong reduction of both k_{f} and k_{nr} such that the quantum yields remain sufficiently high in polar solvents, thereby providing the basis for the use of **6a** as fluorescent probe.[68] Such a photophysically interesting and rarely found anti-energy gap law behavior indicates photochemical and/or conformational changes in the excited state.[80,81] A possible explanation could involve a conical intersection with the ground state, i.e., a "photochemical funnel" where the access from the S_1 to the S_0 state is extremely fast.[82] If such a conical intersection is close to the starting conformation, it induces large nonradiative decay constants. If it is more difficult to reach from the perpendicular conformation after excited-state relaxation, the nonradiative decay rate can decrease although the energy gap to the ground state is smaller, corresponding to red shifted fluorescence (see section 3.1, behavior of **4** and **5** in apolar solvents with respect to polar solvents). This results in an anti-energy gap law behavior. If the relaxed conformation, however, reveals much larger nonradiative rate constants than the starting conformation as is the case for acceptor-protonated **3** and **4** (see, e.g., the strong reduction in fluorescence quantum yield for these species in Table 5), this leads to the normal energy gap behavior.

*Spectroscopic Properties of Charged bpb-R **1**–**5** within the Framework of Neutral and Ionic D–A Biphenyls.* As has been derived in section 3.3, the most intriguing spectroscopic features of charged bpb-R are (i) strongly red shifted and clearly distinguishable emission bands of **2**⊂H⁺ and **2**⊂2H⁺ as well as **3**⊂H⁺ and **3**⊂2H⁺, (ii) a very strong dependence of the fluorescence quantum yields on the donor strength of the substituent R for A-protonated bpb-R, (iii) comparatively high fluorescence quantum yields, small k_{f}, and small k_{nr} values for A-protonated **2**, and (iv) high fluorescence quantum yields and high k_{f} values for completely protonated **4** and **1**.

The spectroscopic features of charged bpb-R are to a large extent determined by the transformation of the already strong acceptor terpyridine into an even stronger cationic acceptor upon protonation or alkylation and the donor strength of R. The analyte-induced increase in acceptor strength yields the desired analytically favorable red shifts of the absorption and emission bands of the bpb-R family in polar solvents, at least for **2**–**5** and monoprotonated **1** as revealed in section 3.3. Similarly to, e.g., (neutral) **7**/(ionic) **8**[75] and aryl-substituted tropyliums ions,[76] the size of both the fluorescence quantum yields and the k_{f} values of A-protonated and A-alkylated bpb-R are mainly governed by the analyte- or charge-induced change of the relative energetic positions and rate constants of the competing reactions of the excited species involved, i.e., a planar strongly emissive CT species and a more relaxed, considerably less emissive twisted CT species; see sections 3.3. and 3.4.[36] The small radiative rate constants and the lack of a detectable emission in the case of A-protonated **4** indicate the formation of a CT state of twisted conformation in highly polar solvents for all the protonated and alkylated species derived from **2**, **3**, and **4**. Nevertheless, the fluorescence quantum yields of protonated and alkylated **2** and even of monoprotonated **3** are still high in comparison to those of other ionic D–A biphenyls with an unbridged aryl–aryl bond. For instance, they considerably exceed that of **8** substituted with a DMA group in equipolar, but protic ethanol ($\phi_{\mathrm{f}} = 8 \times 10^{-3}$)[75] despite the comparable energetic positions of the emission bands of monoprotonated **3** and **8**. This comparison can, however, be hampered by proticity quenching contributing to the very weak emission of **8**. Intriguing is the strong reduction of the nonradiative rate constants of protonated and alkylated **2** by a factor of ca. 7 compared to neutral **2** in combination with the strongly red
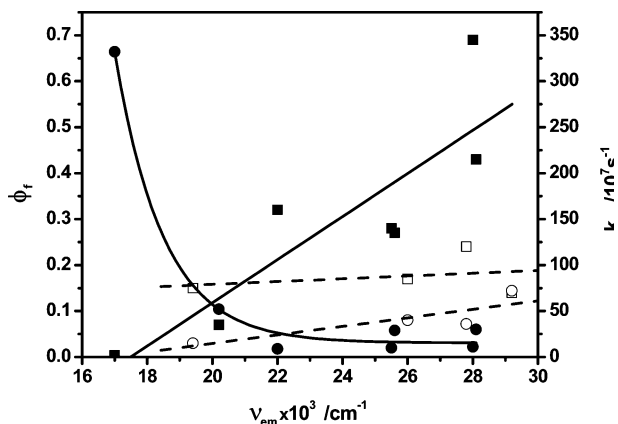
Figure 10. Fluorescence quantum yield, ϕ_f, and nonradiative rate constant, k_{nr}, of neutral (open symbols) and protonated (filled symbols) bpb-R as a function of the spectral position of the respective emission maximum. ϕ_f neutral (open square), ϕ_f protonated (filled squares), k_{nr} neutral (open circles), and k_{nr} protonated (filled circles). The lines are only guides for the eye.

shifted emission spectra (see Table 6). This behavior is similar to that of **4** and **5** (see section 3.1 and Table 3), where k_{nr} is decreased, e.g., in highly polar acetonitrile compared to apolar cyclohexane, although switching to an emissive TICT conformation with bathochromically shifted fluorescence occurs. Obviously, monoprotonated and doubly protonated **2** also present exceptions to the energy gap rule.

The influence of the CT character of the species formed and thus, for a given acceptor, the influence of the donor strength of R on the size of k_{nr} within the bpb-R series is summarized in Table 6 and section 3.3. This dependence most likely accounts for the absence of fluorescence from A-protonated **4**. For this species, the radiative rate is expected to be very small and the nonradiative one very large due to the protonation-induced further narrowing of the S_0–S_1 gap as suggested by the spectroscopic properties of monoprotonated and doubly protonated **3**. A similar observation has been made, e.g., for dimethylamino pyridine or pyrimidine,[83] where alkylation leads to the disappearance of fluorescence. Simultaneous protonation of both donor and acceptor receptors of bpb-DMA and bpb-A15C5, however, yields a strongly emissive species, the spectral properties of which resemble those of bpb-H. The high k_f values are indicative of emission from an allowed planar CT state. This is also true for completely protonated **1**.

3.6. Analytical Potential of bpb-R as Fluorescent Probes and Molecular Switches. *Potential as Fluorescent Probes.* Ratiometric emission sensing with D–A substituted sensor molecules relies on the formation of emissive acceptor chelates. The corresponding structure–property relation for neutral and ionic bpb-R is highlighted in Figure 10, which summarizes the dependence of the fluorescence quantum yields and nonradiative rate constants of these molecules on the spectral position of the emission maximum. The latter is a direct measure for the CT character of the neutral and protonated fluorescent probes of the bpb-R series. We depict both the fluorescence quantum yield and k_{nr} in Figure 10 as the signal- or output-controlling fluorescence quantum yield is governed by the size of both k_f revealing the nature and allowance of the optical transition and the competing k_{nr}. The magnitude of k_{nr} provides a tool to distinguish between conventional energy gap behavior and rare anti-energy gap rule behavior. As is evident from Figure 10, moderately fluorescent acceptor chelates with red shifted emission spectra and fluorescence quantum yields on the order of 0.05–0.30 result only for weak acceptors such as CF$_3$ as

well as weak and medium donors like H and OMe. In the case of **3**, this is only valid for the monoprotonated species. The main factor governing the photophysics of these members of the bpb-R series is the reduction in k_{nr} that compensates for the decrease in k_f linked to the A-protonation-induced switching from LE to TICT population. This analytically favorable effect is most pronounced for **2**. Interestingly, this behavior deviates from the spectroscopic properties of the bifunctional sensor molecule **9** (see Scheme 3) and its monocoordinated analogues recently investigated by us.[26] Although the coordination-induced transformation of this D–D biphenyl into a D–A biphenyl is accompanied by a fluorescence enhancement for protons and, e.g., zinc, calcium, and mercury ions, this effect is due to both an increase in k_f and a slight decrease in k_{nr}. Obviously, in the case of **2**, protonation-induced planarization and rigidization of the terpyridine fragment seem to contribute to the strong decrease in k_{nr}.[21,72] This assumption can also explain the higher k_{nr} values and accordingly smaller fluorescence quantum yield of bisalkylated **2** compared to **2**⊂2H$^+$ (see Table 6), where the alkylation of the 2- and 6-pyridine groups sterically hinders and prevents the planarization of the terpyridine moiety.[63] Accordingly, even more favorable fluorescence effects can be anticipated upon cation chelation of bpb-R as metal ion binding of the terpyridine acceptor supposedly introduces a smaller charge into the terpyridine moiety of bpb-R compared to protonation—and thus a smaller change in acceptor strength and D–A character—and simultaneously strongly enhances its rigidity. In the case of protonated **3** with its medium-sized donor substituent and CT character, the potentially fluorescence-enhancing planarization and rigidization of the terpyridine moiety can compete with the strong tendency toward formation of a forbidden CT state of twisted conformation initiated by the strong cationic acceptor partly for **3**⊂H$^+$, but not for **3**⊂2H$^+$, as revealed by both the considerable reduction in k_f and the strong increase in k_{nr} for this species; see Table 6 and Figure 10. The same holds for members of the bpb-R family where the TICT state is the lowest energy minimum for both the neutral and A-protonated state, such as **4** and **5**. In this case, the k_{nr} values are small for the neutral species but large for the protonated one, such that the acceptor chelates are barely emissive. This, however, provides the basis for the analytically interesting ON–OFF–ON switching of the fluorescence upon transformation of neutral bpb-R into A-coordinated and A- and D-coordinated bpb-R.

The strong spectroscopic effects accompanying A-protonation of bpb-H and bpb-OMe enable true ratiometric emission sensing and the spectroscopic communication of the states/inputs *nonprotonated/no protons*, *monoprotonated/few protons*, and *double protonated/many protons* by proper choice of absorption, excitation, and emission wavelengths. For instance, for the fluorescent sensor molecule **3**, an emission signal at 380 nm is representative for *none*, an emission signal at 530 nm is representative for *few*, and one at 670 nm is representative for *many protons*, respectively. In the case of **2**, where the emission bands of the unprotonated and monoprotonated species more strongly overlap as compared to **3**, additional selectivity can be gained from time-resolved-fluorescence measurements. The lifetimes of 1.2 and 7.0 ns found for **2** and **2**⊂H$^+$ (see Table 6) allow a clear distinction between both species. For **1**, the spectral differences between the unprotonated probe and its monoprotonated and completely protonated analogues as well as the differences in fluorescence lifetime are not strong enough to allow for a clear distinction between these species.

For the eventual use of biphenyl-type molecules as fluorescent sensors, bpb-H and bpb-OMe with their strong monoprotonation

and double protonation-induced red shifts in emission can be developed into analytically attractive systems, for instance by the introduction of substituents that enhance their water solubility. Furthermore, the methoxy group can be turned into or exchanged for a cation-responsive receptor such as a benzo crown or a thiaoxa crown.[84] To realize the formation of moderately emissive acceptor chelates for biphenyl-type molecules substituted with strong donors such as DMA or A15C5, a pH- and/or cation-responsive acceptor with a decreased acceptor strength compared to terpyridine is mandatory. An obvious approach here is the introduction of donor-type substituents at the 2-position and 6-position of the central pyridine ring to reduce and fine-tune its acceptor strength. For application as fluorescent probes for metal ions, such substituents should contain heteroatoms such as sulfur atoms as additional cation binding sites to also tune the analyte selectivity of the A-type receptor.[85] One strategy currently investigated by us focuses here on 2- and 6-thienyl substituents.[69]

Bifunctionality of bpb-R. bpb-DMA and bpb-A15C5 and related molecules are attractive candidates for bimodal fluorescence signaling. As follows, e.g., from Figures 6 and 7, acceptor coordination and the simultaneous engagement of both D- and A-receptors in analyte binding yield species that clearly differ from each other in energy and intensity in absorption and emission as well as in fluorescence lifetime. Taking as an example compound **4**, the red, yet moderate emission of the parent ligand and the A-protonation-induced appearance of a new absorption band are encouraging, as is the formation of a strongly emissive species with blue shifted absorption and emission spectra upon simultaneous engagement of both donor and acceptor receptors. These effects are much more favorable with respect to multimodal optical communication as the results of the protonation and cation coordination experiments recently performed by us with bifunctional **9** revealing a very weak blue shifted emission upon protonation of both binding sites and a complete lack of emission for double coordination to metal ions.[26] Moreover, these effects are promising not only for bimodal pH-sensing (see, e.g., Figure 7), but also for the design of bifunctional cation-responsive fluorescent probes that form spectroscopically distinguishable three-state (one analyte, two concentration regimes) or four-state (two different analytes) systems.[48]

Potential as Molecular Switches and Logic Gates. An exciting extension of fluorescent sensor studies has been the development of molecular switches and molecular equivalents of logic gates and the implementation of these devices in molecular arithmetics.[1,86,87] Molecular switches and logic gates both convert input stimulations into output signals with intrinsic protocols following the principles of binary logic.[86] In the case of the former, this requires proper assignment of threshold values and logic conventions to their input and output signals. A number of different systems including, e.g., YES,[88] NOT,[89] AND,[90] OR,[91] NOR,[92] and INHIBIT[92,93] logic gates have been reported. At present, the majority of these devices respond to combinations of protons and alkali or alkaline earth metal ions and are ET-operated, i.e., undergo intensity alterations.[33,94] Here, however, true ON–OFF or OFF–ON switching, i.e., switching between a nonfluorescent and a highly fluorescent state—though naturally preferred—is often not achieved. Examples for CT-operated logic gates that yield spectrally distinguishable species and principally offer different output signals are comparatively rare.[28,34] In any case, systems are of interest that display clearly distinguishable changes of different measurable optical parameters specific for certain chemical inputs. Advantageous in this

respect are the strong input-controlled changes in intensity and energy in absorption and fluorescence as well as in fluorescence lifetime generated by the bpb-R sensor molecules providing different output signals that can be separately read out. However, as the protonation studies presented by us reveal only the inputs *no*, *little*, and *many* with the latter two inputs being not separable within the typically used logic convention,[86,94] we can only estimate their potential. For instance, bpb-DMA communicates A-protonation via formation of a new strongly red shifted absorption band at 467 nm and disappearance of the ligand's emission band at 546 nm and A- and D-protonation via disappearance of the A-chelate's absorption band at 467 nm and appearance of a new blue shifted and strong emission band at 356 nm; see Figure 7. Accordingly, it provides principally three simple outputs as well as true OFF–ON–OFF switching in absorption (470 nm; inputs *no*, *little*, *many* and outputs *0*, *1*, *0* with *1* and *0* equaling high and low intensity) and, more importantly, ON–OFF–OFF (550 nm; inputs *no*, *little*, *many* and outputs *1*, *0*, *0*) and OFF–OFF–ON (350 nm; inputs *no*, *little*, *many* and outputs *0*, *0*, *1*) switching in fluorescence for two different emission wavelengths and a single excitation wavelength. Within the typically used framework of logic gate assignment, bpb-DMA, e.g., presents a NOT logic gate with respect to the input *protons* and the output *(high) emission at 550 nm* using a positive logic convention.[86] This is also true for instance for bpb-OMe and the input *protons* and the output *(high) emission at 390 nm*.

4. Summary and Conclusion

On the basis of bpb-R molecules substituted with integrated electron-accepting terpyridine receptors and coordinating and noncoordinating donors, we developed a family of simple monofunctional and bifunctional CT-operated fluorescent probes. These compounds are capable of ratiometric emission sensing of protons and bimodal pH signaling in a coordination-site-specific fashion. The photophysics of these sensor molecules and their protonated analogues are governed by the molecule's CT character, i.e., a CT-controlled excited-state barrier toward relaxation to a CT state of forbidden nature and a CT-controlled switching between anti-energy and energy gap law type behavior. This provides the basis for analytically favorable red shifted emission spectra in combination with comparatively high fluorescence quantum yields for bpb-DMA and bpb-A15C5 and especially for monoprotonated and doubly protonated bpb-H by a strong reduction in k_{nr} that compensates for the decrease in k_f linked to the emission from a CT state of twisted conformation. For neutral and charged bpb-R, the prerequisite for large k_f and accordingly a moderate to strong emission from an allowed planar CT state is a weak D–A character as conceived for bpb-CF$_3$ and bpb-H as well as for D- and A-protonated bpb-CF$_3$ and bpb-DMA. The photophysical processes involved in the excited-state relaxation of bpb-R enable communication of analyte coordination in a binding-site-specific mode with the parent ligand and the acceptor-coordinated compound(s)—and in the case of bpb-DMA and bpb-A15C5 also the A- and D-coordinated probe—differing in energy and intensity of their absorption and fluorescence bands as well as in fluorescence lifetime. This provides an elegant tool for the simple distinction between the inputs *no protons*, *few protons*, and *many protons* and thus an extended dynamic range for protons employing bpb-H and bpb-OMe as well as bpb-DMA.

Supporting Information Available: Emission spectra of bpb-OMe and pbp-DMA in solvents of different polarities and proticities and a comparison of the absorption and emission spectra of neutral and protonated bpb-CF$_3$ and bpb-H. This material is available free of charge via the Internet at http://pubs.acs.org.

References and Notes

(1) *Molecular Switches*; Feringa, B. L., Ed.; Wiley-VCH GmbH: Weinheim, 2001.

(2) Special issue on Luminescent Sensors. *Coord. Chem. Rev.* **2000**, *205*.

(3) de Silva, A. P.; Gunaratne, H. Q. N.; Gunnlaugson, T.; Huxley, A. J. M.; McCoy, C. P.; Rademacher, J. T.; Rice, T. E. *Chem. Rev.* **1997**, *97*, 1515.

(4) Beer, P. D.; Gale, P. A. *Angew. Chem., Int Ed.* **2001**, *40*, 486. Martínez-Máñez, R.; Sancenón, F. *J. Fluoresc.* **2005**, *15*, 267.

(5) For example: Beer, P. D.; Cadman, J. *Coord. Chem. Rev.* **2000**, *205*, 131. Beer, P. D.; Gale, P. A.; Chen, G. Z. *Coord. Chem. Rev.* **1999**, *185–186*, 3 and references therein.

(6) Engeser, M.; Fabbrizzi, L.; Licchelli, M.; Sacchi, D. *Chem. Commun.* **1999**, 1191. Herranz, M. A.; Martín, N.; Ramey, J.; Guldi, D. M. *Chem. Commun.* **2002**, 2968.

(7) For example: Irie, M. *Chem. Rev.* **2000**, *100*, 1685. Tyson, D. S.; Bignozzi, C. A.; Castellano, F. N. *J. Am. Chem. Soc.* **2002**, *124*, 4562. Fernandez-Acebes, A.; Lehn, J.-M. *Eur. Chem. J.* **1999**, *5*, 3285. Giordano, L.; Jovin, T. M.; Irie, M.; Jares-Erijman, E. A. *J. Am. Chem. Soc.* **2002**, *124*, 7481. Guo, X.; Zhang, D.; Wang, T.; Zhu, D. *Chem. Commun.* **2003**, 914.

(8) Irie, M.; Fukaminato, T.; Saski, T.; Tamai, N.; Kawai, T. *Nature* **2002**, *420*, 759. Cinelli, R. A. G.; Pellegrini, V.; Ferrari, A.; Faraci, P.; Nifosi, R.; Tyagi, M.; Giacca, M.; Beltram, F. *Appl. Phys. Lett.* **2001**, *79*, 3353. La Clair, J. J. *Angew. Chem., Int. Ed.* **1999**, *38*, 3045. Zang, L.; Liu, R.; Holman, M. W.; Nguyen, K. T.; Adams, D. M. *J. Am. Chem. Soc.* **2002**, *124*, 10640.

(9) Wiegmann, T. B.; Welling, L. W.; Beatty, D. M.; Howard, D. E.; Vamos, S.; Morris, S. J. A. *J. Physiol.* **1993**, *265*, C1184. Salvador, J. M.; Inesi, G.; Rigaud, J. L.; Mata, A. M. *Biol. Chem.* **1998**, *273*, 18230. Vo-Dinh, T.; Viallet, P.; Ramirez, L.; Pal, A.; Vigo, J. *Anal. Chim. Acta* **1994**, *295*, 67. Hirshfeld, K. M.; Toptygin, D.; Grandhige, G.; Packard, B. Z.; Brand, L. *Biophys. Chem.* **1998**, *71*, 63.

(10) *Advanced Concepts in Fluorescence Spectroscopy, Part A: Small Molecule Sensing*; Geddes, C. D., Lakowicz, J. R., Eds.; Topics in Fluorescence Spectroscopy 9; Springer Science + Business Media Inc.: New York, 2005.

(11) See, for example: Rurack, K.; Resch-Genger, U. *Chem. Soc. Rev.* **2002**, *31*, 116 and references therein.

(12) Rurack, K. *Spectrochim. Acta, Part A* **2001**, *57*, 2161 and references therein.

(13) Rudolf, R.; Mongillo, M.; Rizzuto, R.; Pozzan, T. *Nat. Rev.* **2003**, *4*, 579.

(14) Fages, F.; Desvergne, J.-P.; Bouas-Laurent, H.; Marsau, P.; Lehn, J.-M.; Kotzyba-Hibert, F.; Albrecht-Gary, A.-M.; Al-Joubbeh, M. *J. Am. Chem. Soc.* **1989**, *111*, 8672. Cho, H. K.; Lee, D. H.; Hong, J.-I. *Chem. Commun.* **2005**, 1690. Bouas-Laurent, H.; Castellan, A.; Daney, M.; Desvergne, J.-P.; Guinand, G.; Marsau, P.; Riffaud, J. *J. Am. Chem. Soc.* **1986**, *108*, 315. Desvergne, J.-P.; Bouas-Laurent, H.; Perez-Inestrosa, E.; Marsau, P.; Cotrait, M. *Coord. Chem. Rev.* **1999**, *185–186*, 357. Suzuki, Y.; Morozumi, T.; Nakamura, H.; Shimomura, M.; Hayashita, T.; Bartsh, R. A. *J. Phys. Chem. B* **1998**, *102*, 7910. Bencini, A.; Bianchi, A.; Lodeiro, C.; Masotti, A.; Parola, J.; Pina, F.; de Melo, J. S.; Valtancoli, V. *Chem. Commun.* **2000**, 1639. Yang, J.-S.; Lin, C.-S.; Hwang, C.-Y. *Org. Lett.* **2001**, *3*, 889. Liu, Y.; Duan, Y.; Zhang, H.-Y.; Jiang, X.-L.; Han, J.-R. *J. Org. Chem.* **2005**, *70*, 1450. Sankaran, N. B.; Nishizawa, S.; Watanabe, M.; Uchida, T.; Teramae, N. *J. Mater. Res.* **2005**, *15*, 2755. Hennrich, G.; Walther, W.; Resch-Genger, U.; Sonnenschein, H. *Inorg. Chem.* **2001**, *40*, 641. Yang, J.-S.; Lin, C.-S.; Hwang, C.-Y. *Org. Lett.* **2001**, *3*, 889.

(15) Another though comparatively rarely employed strategy toward ratiometric sensing is sensor molecules equipped with two different chromophores, such as a cyclam substituted with a pyrene and a NBD fluorophore (see Kim, S. H.; Kim, J. S.; Park, S. M.; Chang, S.-K. *Org. Lett.* **2006**, *8*, 371), or a fluorescent probe for dual wavelength imaging based on Cy5.5 and Cy7 (see Kirchner, M. F.; Weissleder, R.; Josephson, L. *Bioconjugate Chem.* **2004**, *15*, 242).

(16) Kollmannsberger, M.; Rurack, K.; Resch-Genger, U.; Daub, J. *J. Phys. Chem. B* **1998**, *102*, 10211. Rurack, K.; Kollmannsberger, M.; Resch-Genger, U.; Daub, J. *J. Am. Chem. Soc.* **2000**, *122*, 968. Wu, F.-Y.; Li, Z.; Wen, Z.-C.; Zhou, N.; Zhao, Y.-F.; Jiang, Y.-B. *Org. Lett.* **2002**, *4*, 3203. Letard, J.-F.; Delmond, S.; Lapouyade, R.; Braun, D.; Rettig, W.; Kreissler, M. *Recl. Trav. Chim. Pays-Bas* **1995**, *114*, 517. Malval, J. P.; Lapouyade, R.; Leger J. M.; Jarry, C. *Photochem. Photobiol. Sci.* **2003**, *2*, 259. Malval, J. P.; Lapouyade, R. *Helv. Chim. Acta* **2001**, *84*, 2439. Mello, J. V.; Finney, N. S. *Angew. Chem.* **2001**, *113*, 1584. Kiyose, K.; Kojima, H.; Urano, Y.; Nagano, T. *J. Am. Chem. Soc.* **2006**, *128*, 6548.

(17) Cheng, C. J.; Jaworski, J.; Nolan, E. M.; Sheng, M.; Lippard, S. J. *Proc. Natl. Acad. Sci. U.S.A.* **2004**, *101*, 1129.

(18) Ros-Lis, J. V.; Marcos, D.; Martinez-Manez, R.; Rurack, K.; Soto, V. *Angew. Chem., Int. Ed.* **2005**, *44*, 4405.

(19) An alternative strategy omitted here is molecules equipped with a fluorophore, the emission spectrum of which is extremely sensitive to the polarity of the local environment. See, for example: Deo, S.; Arnold Godwin, H. *J. Am. Chem. Soc.* **2000**, *122*, 174.

(20) Adam, S. R.; Kao, J. P. Y.; Grynkiewicz, G.; Minta, A.; Tsien, R. Y. *J. Am. Chem. Soc.* **1988**, *110*, 3212. Martin, M. M.; Plaza, P.; Hung, D.; Meyer, Y. H. *Chem. Phys. Lett.* **1993**, *202*, 425. Mathevet, R.; Jonusauskas, G.; Rullière, C.; Létard, J.-F.; Lapouyade, R. *J. Phys. Chem.* **1995**, *99*, 15709. Martin, M. M.; Plaza, P.; Meyer, Y. H. *Chem. Phys.* **1995**, *192*, 367. Martin, M. M.; Plaza, P.; Meyer, Y. H.; Badaoui, F.; Bourson, J.; Lefevre, J.-P.; Valeur, B. *J. Phys. Chem.* **1996**, *100*, 6879. Plaza, P.; Leray, I.; Changenet-Barret, P.; Martin, M. M.; Valeur, B. *ChemPhysChem* **2002**, *3*, 668.

(21) Goodall, W.; Williams, J. A. G. *Chem. Commun.* **2001**, 2514.

(22) Bricks, J. L.; Slominskii, J. L.; Kudinova, M. A.; Tolmachev, A. I.; Rurack, K.; Resch-Genger, U.; Rettig, W. *J. Photochem. Photobiol., A* **2000**, *132*, 193.

(23) Wen, Z.-C.; Yang, R.; He, H.; Jiang, Y.-B. *Chem. Commun.* **2006**, 106.

(24) For example, see: Bourson, J.; Pouget, J.; Valeur, B. *J. Phys. Chem. A* **1993**, *97*, 4552. Leray, I.; Habib-Jiwan, J.-L.; Branger, C.; Soumillion, J.-Ph.; Valeur, B. *J. Photochem. Photobiol., A* **2000**, *132*, 163.

(25) Malval, J.-P.; Lapouyade, R. *Chem. Commun.* **2000**, 289. Delmond, S.; Létard, J.-F.; Lapouyade, R.; Mathevet, R.; Jonusauskas, G.; Rullière, C. *New J. Chem.* **1996**, *20*, 861. Costero, A. M.; Sanchis, J.; Gil, S.; Sanz, V.; Williams, J. A. G. *J. Mater. Res.* **2005**, *15*, 2850.

(26) Li, Y. Q.; Bricks, J. L.; Resch-Genger, U.; Spieles, M.; Rettig, W. *J. Fluoresc.* **2006**, *16*, 337.

(27) Fery-Forgues, S.; Le Bris, M. T.; Guette, J.-P.; Valeur, B. *J. Phys. Chem.* **1988**, *92*, 6233. Fery-Forgues, S.; Le Bris, M. T.; Mialocq, J.-C.; Pouget, J.; Rettig, W.; Valeur, B. *J. Phys. Chem.* **1992**, *96*, 701. Rurack, K.; Rettig, W.; Resch-Genger, *Chem. Commun.* **2000**, 407. Marcotte, N.; Plaza, P.; Lavabre, D.; Fery-Forgues, S.; Martin, M. M. *J. Phys. Chem. A* **2003**, *107*, 2394. Marcotte, N.; Fery-Forgues, S.; Lavabre, D.; Marguet, S.; Pivarenko, V. G. *J. Phys. Chem. A* **1999**, *103*, 3163.

(28) Rurack, K.; Koval'chuck, A.; Bricks, J. L. *J. Am. Chem. Soc.* **2001**, *123*, 6205.

(29) de Silva, A. P.; Fox, D. B.; Moody, T. S.; Weir, S. M. *Trends Biotechnol.* **2001**, *19*, 29. Brown, G. J.; de Silva, A. P.; Pagliari, S. *Chem. Commun.* **2002**, 2461. de Silva, A. P.; McClenaghan, N. D. *Chem.—Eur. J.* **2002**, *8*, 4935. Guo, X.; Zhang, D.; Zhu, D. *Adv. Mater.* **2004**, *16*, 125.

(30) Resch-Genger, U.; Hennrich, G. Redox-switchable Fluorescent Sensors. In *Advanced Concepts in Fluorescence Spectroscopy, Part A: Small Molecule Sensing*; Geddes, C. D., Lakowicz, J. R., Eds.; Topics in Fluorescence Spectroscopy 9; Springer Science + Business Media Inc.: New York, 2005, and references therein.

(31) Wilson, J. N.; Bunz, U. H. F. *J. Am. Chem. Soc.* **2005**, *127*, 4124.

(32) Brumbaugh, J.; Schleifenbaum, A.; Gasch, A.; Sattler, M.; Schultz, C. *J. Am. Chem. Soc.* **2006**, *128*, 24.

(33) For example, see: de Silva, A. P.; McClenaghan, N. D. *J. Am. Chem. Soc.* **2000**, *122*, 3965. Ji, H.-F.; Dabestani, R.; Brown, G. M. *J. Am. Chem. Soc.* **2000**, *122*, 9306. Iwata, S.; Tanaka, K. *J. Chem. Soc., Chem. Commun.* **1995**, 1491. de Silva, A. P.; McClenaghan, N. D. *Chem.—Eur. J.* **2004**, *10*, 574. Koskela, S. J. M.; Fyles, T. M.; James, T. D. *Chem. Commun.* **2005**, 945. Xu, X.; Xu, H.; Ji, H.-F. *Chem. Commun.* **2001**, 2092. de Silva, S. A.; Amorelli, B.; Isidor, D. C.; Loo, K. C.; Crooker, K. E.; Pena, Y. E. *Chem. Commun.* **2002**, 1360.

(34) Rurack, K.; Bricks, J. L.; Schulz, B.; Maus, M.; Reck, G.; Resch-Genger, U. *J. Phys. Chem. A* **2000**, *104*, 6171.

(35) de Silva, A. P.; Dixon, I. M.; Gunaratne, H. Q. N.; Gunnlaugsson, T.; Maxwell, P. R. S.; Rice, T. E. *J. Am. Chem. Soc.* **1999**, *121*, 1393. Bag, B.; Bharadwaj, P. K. *Chem. Commun.* **2005**, 513.

(36) Maus, M.; Rettig, W.; Bonafoux, D.; Lapouyade, R. *J. Phys. Chem. A* **1999**, *103*, 3388.

(37) Maus, M.; Rettig, W. *J. Inf. Rec.* **1998**, *24*, 461. Maus, M.; Rettig, W. *Chem. Phys.* **1997**, *218*, 151. Maus, M.; Rettig, W.; Lapouyade, R. *J. Inf. Rec.* **1996**, *22*, 451.

(38) Lahmani, F.; Breheret, E.; Zehnacker-Rentien, A.; Amatore, C.; Jutand, A. *J. Photochem. Photobiol., A* **1993**, *70*, 39.

(39) Herbich, J.; Waluk, J. *Chem. Phys.* **1994**, *188*, 247.

(40) Chou, P. T.; Chang, C. P.; Clements, J. H.; Meng-Shin, K. *J. Fluoresc.* **1995**, *5*, 369.

(41) Ephardt, H.; Fromherz, P. *J. Phys. Chem.* **1991**, *95*, 6792. Fromherz, P.; Heilemann, A. *J. Phys. Chem.* **1992**, *96*, 6864. Röcker, C.; Heilemann, A.; Fromherz, P. *J. Phys. Chem.* **1996**, *100*, 12172.

(42) TICT: twisted intramolecular charge transfer. See, for example: Rettig, W. *Top. Curr. Chem.* **1994**, *169*, 253.

(43) For example, see: Cargill Thompson, A. M. W. *Coord. Chem. Rev.* **1997**, *160*, 1. Lohmeijer, B. G. G.; Schubert, U. S. *Macromol. Chem. Phys.* **2003**, *204*, 1072. Newkome, G. R.; Yoo, K. S.; Moorefield, C. N. *Chem. Commun.* **2002**, 2164. Berthet, J. C.; Riviere, C.; Miquel, Y. *Eur. J. Inorg. Chem.* **2002**, 1439. Holland, J. M.; Liu, X. M.; Zhao, J. P. *J. Chem. Soc., Dalton. Trans.* **2000**, 3316. Janini, T. E.; Fattore, J. L.; Mohler, D. L. *J. Organomet. Chem.* **1999**, *578*, 260. Mürner, H.-R.; Chassat, E.; Thummel, R. P.; Bünzli, J.-C. G. *J. Chem Soc., Dalton Trans.* **2000**, 2809.

(44) Ballardini, V.; Balzani, V.; Clemente-Leon, M. *J. Am. Chem. Soc.* **2002**, *124*, 12786. Laine, P.; Bedioui, F.; Ochsenbein, P.; Marvaud, V.; Bonin, M.; Amouyal, E. *J. Am. Chem. Soc.* **2002**, *124*, 1364. Flamini, L.; Barigelletti, F.; Armaroli, N.; Collin, J.-P.; Dixon, I. M.; Sauvage, J. P.; Williams, J. A. G. *Coord. Chem. Rev.* **1999**, *192*, 671. Wang, X.-Y.; Del Guerzo, A.; Schmehl, R. H. *Chem. Commun.* **2002**, 2344. Hofmeier, H.; Schubert, U. S. *Chem. Soc. Rev.* **2004**, *33*, 373.

(45) See, for example: Padilla-Tosta, M. E.; Lloris, J. M.; Martinez-Manez, R. *Eur. J. Inorg. Chem.* **2001**, 1475. Ziessel, R. *J. Inclusion Phenom. Macrocyclic Chem.* **1999**, *35*, 369. Whittle, B.; Batten, S. R.; Jeffery, J. C.; Rees, L. H.; Ward, M. D. *J. Chem. Soc., Dalton Trans.* **1996**, 4249. Al Shihadeh, Y.; Benito, A.; Lloris, J. M.; Martinez-Manez, R.; Soto, J. *Transition Met. Chem.* **2002**, *27*, 307. Barigletti, F.; Flamigni, L.; Calogero, G.; Hammarström, L.; Sauvage, J. P.; Collin, J.-P. *Chem. Commun.* **1998**, 2333. Goodall, W.; Williams, J. A. G. *J. Chem. Soc., Dalton Trans.* **2000**, 2893. Yam, V. W.-W.; Lee, V. W.-M. *J. Chem. Soc., Dalton Trans.* **1997**, 3005. Licini, M.; Williams, J. A. G. *Chem. Commun.* **1999**, 1943. Che, C.-M.; Zhang, J.-L.; Lin; L.-R. *Chem. Commun.* **2002**, 2556. de Silva, A. P.; Gunaratne, H. Q. N.; Rice, T. E.; Stewart, S. *Chem. Commun.* **1997**, 1891. Tang, W.-S.; Lu, X.-X.; Wong, K. M.-C.; Yam, V. W.-W. *J. Mater. Chem.* **2005**, *15*, 2714.

(46) Buschel, M.; Helldobler, M.; Daub, J. *Chem. Commun.* **2002**, 1338.

(47) Constable, E. C.; Smith, D. R. *Supramol. Chem.* **1994**, *4*, 5. Albano, G.; Balzani, V.; Constable, E. C.; Maestri, M.; Smith, D. R. *Inorg. Chim. Acta* **1998**, *277*, 225. Fabre, B.; Lehmann, U.; Schlüter, A. D. *Electrochim. Acta* **2001**, *46*, 2855. Akasaka, T.; Otsuki, J.; Araki, K. *Chem.−Eur. J.* **2002**, *8*, 130.

(48) Li, Y. Q.; Bricks, J. B.; Resch-Genger, U.; Spieles, M.; Rettig, W. *J. Phys. Chem. A* **2006**, *110*, 10972.

(49) Resch-Genger, U.; Pfeifer, D.; Monte, C.; Pilz, W.; Hoffmann, A.; Spieles, M.; Rurack, K.; Hollandt, J.; Taubert, D.; Schönenberger, B.; Nording, P. *J. Fluoresc.* **2005**, *15*, 315.

(50) Pfeifer, D.; Hoffmann, K.; Hoffmann, A.; Monte, C.; Resch-Genger, U. *J. Fluoresc.* **2006**, *16*, 581.

(51) *Principles of Fluorescence Spectroscopy*, 2nd. ed.; Lakowicz, J. R., Ed.; Kluwer Academic/Plenum Press: New York, 1999.

(52) Demas, J. N. *Optical Radiation Measurements*; Mielenz, K. D., Ed.; Academic Press: New York, 1982; Vol. 3, p 195.

(53) Drexhage, K. H. *J. Res. Natl. Bur. Stand. (U.S.)* **1976**, *80A*, 421.

(54) *Time-Correlated Single-Photon Counting*; Connor, D. V., Phillips, D., Eds.; Academic Press: London, 1984.

(55) Weigel, W.; Rettig, W.; Dekhtyar, M.; Modrakowski, C.; Beinhoff, M.; Schlüter, A. D. *J. Phys. Chem. A* **2003**, *107*, 5941.

(56) Globals Unlimited. Laboratory of Fluorescence Dynamics at the University of Illinois, 1992.

(57) Dewar, M. J. S.; Zoebisch, E. G.; Healy, E. F.; Stewart, J. J. P. *J. Am. Chem. Soc.* **1985**, *107*, 3202.

(58) AMPAC 6.0 and AMPAC 6.55; Semichem. Inc.: Shawnee, 1997.

(59) Frisch, M. J.; Trucks, G. W.; Schlegel, H. B.; Gill, P. M. W.; Johnson, B. G.; Robb, M. A.; Cheeseman, J. R.; Keith, T.; Petersson, G. A.; Montgomery, J. A.; Raghavachari, K.; Al-Laham, M. A.; Zakrzewski, V. G.; Ortiz, J. V.; Foresman, J. B.; Cioslowski, J.; Stefanov, B. B.; Nanayakkara, A.; Challacombe, M.; Peng, C. Y.; Ayala, P. Y.; Chen, W.; Wong, M. W.; Andres, J. L.; Replogle, E. S.; Gomperts, R.; Martin, R. L.; Fox, D. J.; Binkley, J. S.; Defrees, D. J.; Baker, J.; Stewart, J. P.; Head-Gordon, M.; Gonzalez, C.; Pople, J. A. *Gaussian 98*, revision A.7; Gaussian, Inc.: Pittsburgh, PA, 1998.

(60) Moya, S. A.; Pastene, R.; Le Bozec, H.; Baricelli, P. J.; Pardey, A. J.; Gimeno, J. *Inorg. Chim. Acta* **2001**, *312*, 7.

(61) Spahni, W.; Calzagerri, G. *Helv. Chim. Acta* **1984**, *67*, 450.

(62) Mutai, T.; Cheon, J.-D.; Arita, S.; Araki, K. *J. Chem. Soc., Perkin Trans. 2* **2001**, 1045.

(63) Schulz, B.; Bricks, J.; Li, Y.-Q.; Resch-Genger, U.; Reck, G. *Acta Crystallogr., Sect. C* **2004**, *60C*, 0402.

(64) Goodall, W.; Wild, K.; Arm, K. J.; Williams, J. A. G. *J. Chem. Soc., Perkin Trans. 2* **2002**, 1669.

(65) Lippert, E. *Z. Naturforsch., A* **1955**, *10a*, 541.

(66) Mataga, N.; Kaifu, Y.; Koizumi, M. *Bull. Chem. Soc. Jpn.* **1956**, *29*, 465.

(67) Karelson, M.; Zerner, M. C. *J. Am. Chem. Soc.* **1990**, *112*, 9405.

(68) Maus, M.; Rurack, K. *New J. Chem.* **2000**, *24*, 677.

(69) Li, Y.-L.; Bricks, J. L.; Resch-Genger, U.; Rettig, W. Manuscript in preparation.

(70) Deng, F.; Kubin, J.; Testa, A. C. *J. Photochem. Photobiol., A* **1998**, *118*, 1. Deng, J.; Testa, A. C. *J. Photochem. Photobiol., A* **1998**, *112*, 191.

(71) Martin, R. B.; Lissfelt, J. A. *J. Am. Chem. Soc.* **1956**, *78*, 938.

(72) Sarkar, A.; Chakravorti, S. *J. Lumin.* **1995**, *63*, 143.

(73) An alternative interpretation, though not favored by us, is that the observed red shifts in absorption and emission may indicate that protonation is easier in the excited state.

(74) Bricks, J. L.; Emmerling, F.; Kharlanov, V.; Kraus, W.; Li, L. Q.; Reck, G.; Resch-Genger, U.; Rettig, W.; Schulz, B. Manuscript in preparation.

(75) Rettig, W.; Kharlanov, V.; Maus, M. *Chem. Phys. Lett.* **2000**, *318*, 173.

(76) Kharlanov, V. A.; Abraham, W.; Rettig, W. *J. Photochem. Photobiol., A* **2001**, *143*, 109.

(77) Grabowski, Z. R.; Rotkiewicz, K.; Rettig, W. *Chem. Rev.* **2003**, *103*, 3899.

(78) Siebrand, W. *J. Chem. Phys.* **1966**, *44*, 4055.

(79) The energy gap law predicts an exponential increase of k_{isc} or k_{nr} with decreasing energy difference between S_1 and the energetically lower lying state, e.g., triplet T_1 or ground state.

(80) Lapouyade, R.; Kuhn, A.; Létard, J. F.; Rettig, W. *Chem. Phys. Lett.* **1993**, *208*, 48.

(81) Letard, J. F.; Lapouyade, R.; Rettig, W. *Chem. Phys.* **1994**, *186*, 119.

(82) Bernardi, F.; Olivucci, M.; Robb, M. A. *Chem. Soc. Rev.* **1996**, *25*, 1321.

(83) Herbich, J.; Grabowski, Z. R.; Woytowicz, H.; Golankiewicz, K. *J. Phys. Chem.* **1989**, *93*, 3439.

(84) Fedorova, O. A.; Fedorov, Y. V.; Vedernikov, A. I.; Gromov, S. P.; Yescheulova, O. V.; Alfimov, M. V.; Woerner, M.; Bossmann, S.; Braun, A.; Saltiel, J. *J. Phys. Chem. A* **2002**, *106*, 6213. Kollmannsberger, M.; Rurack, K.; Resch-Genger, U.; Rettig, W.; Daub, J. *Chem. Phys. Lett.* **2000**, *1−2*, 87.

(85) Constable, E. C.; Henney, R. P. G.; Tocher, D. A. *J. Chem. Soc., Dalton Trans.* **1992**, 2467.

(86) Raymo, F. M. *Adv. Mater.* **2002**, *14*, 401.

(87) Balzani, V.; Credi, A.; Venturi, M. *ChemPhysChem* **2003**, *3*, 49.

(88) de Silva, A. P.; Rupasinghe, R. A. D. D. *J. Chem. Soc., Chem. Commun.* **1985**, 1669.

(89) de Silva, A. P.; Gunnlaugsson, T.; McCoy, C. P. *J. Chem. Educ.* **1997**, *74*, 53.

(90) de Silva, A. P.; Gunaratne, H. Q. N.; McCoy, C. P. *Nature* **1993**, *364*, 42.

(91) de Silva, A. P.; Gunaratne, H. Q. N.; McCoy, C. P. *J. Am. Chem. Soc.* **1997**, *119*, 7891.

(92) de Silva, A. P.; Dixon, I. M.; Gunaratne, H. Q. N.; Gunnlaugsson, T.; Maxwell, P. R. S.; Rice, T. E. *J. Am. Chem. Soc.* **1999**, *121*, 1393.

(93) Gunnlaugsson, T.; MacDonail, D. A.; Parker, D. *J. Am. Chem. Soc.* **2001**, *123*, 12866.

(94) Loiseau, F.; Di Pietro, C.; Campagna, S.; Cavazzini, M.; Marzanni, G.; Quici, S. *J. Mater. Chem.* **2005**, *15*, 2763.